

1

2 **Plant peptidoglycan precursor biosynthesis: Conservation** 3 **between moss chloroplasts and Gram negative bacteria**

4 **Amanda J. Dowson,^{a2} Adrian J. Lloyd,^a Andrew C. Cuming,^b David I. Roper,^a Lorenzo**
5 **Frigerio^a and Christopher G. Dowson^{a3}**

6 ^aSchool of Life Sciences, University of Warwick, Coventry CV4 7AL, United Kingdom

7 ^bCentre for Plant Sciences, University of Leeds, Leeds, LS2 9JT, United Kingdom

8 ¹This work was supported by a Pump Priming Initiative from the University of Warwick.

9 ²Corresponding author

10 ³Senior author

11 A.J.D generated the heterologous expression vectors, prepared and assayed proteins, purified peptidoglycan intermediates
12 from *P. patens* and wrote the manuscript; A.J.L. conceived use of TCA extraction, performed the mass
13 spectrophotometric analysis and analysed the data; A.C.C. assisted with *P. patens* handling; D.I.R. and L.F initiated the
14 enzymatic analysis and Pump Prime funding, C.G.D assisted with funding and A.J.L., D.I.R. and C.G.D. assisted with
15 experimental discussion and critiqued the manuscript.

16 The author responsible for distribution of materials integral to the findings presented in this article in accordance with the
17 policy described in the Instructions for Authors (<https://academic.oup.com/plcell/pages/General-Instructions>) is:

18 A.J.Dowson (a.j.dowson@warwick.ac.uk).

19

20 **Short title:**

21 **Bacterial Peptidoglycan Precursors in Land Plants**

22

23 **Abstract**

24 An accumulation of evidence suggests that peptidoglycan, consistent with a bacterial cell wall, is synthesised around the
25 chloroplasts of many photosynthetic eukaryotes, from glaucophyte algae to land plants at least as evolved as pteridophyte
26 ferns, but the biosynthetic pathway has not been demonstrated. We employed mass spectrometry and enzymology in a
27 twofold approach to characterize the synthesis of peptidoglycan in chloroplasts of the moss *Physcomitrium*
28 (*Physcomitrella*) *patens*. To drive the accumulation of peptidoglycan pathway intermediates, *P.patens* was cultured with

29 the antibiotics phosphomycin, D-cycloserine and carbenicillin, which inhibit key peptidoglycan pathway proteins in
30 bacteria. Mass spectrometry of the TCA-extracted moss metabolome revealed elevated levels of five of the predicted
31 intermediates from UDP-GlcNAc through to the UDP-MurNAc-D,L-diaminopimelate (DAP)-pentapeptide.

32 Most Gram negative bacteria, including cyanobacteria, incorporate *meso*-diaminopimelate (D,L-DAP) into the
33 third residue of the stem peptide of peptidoglycan, as opposed to L-lysine, typical of most Gram positive bacteria. To
34 establish the specificity of D,L-DAP incorporation into the *P.patens* precursors, we analysed the recombinant protein,
35 UDP-MurNAc-tripeptide ligase (*MurE*), from both *P.patens* and the cyanobacterium *Anabaena* sp. strain PCC 7120.
36 Both ligases incorporated D,L-DAP in almost complete preference to L-Lys, consistent with the mass spectrophotometric
37 data, with catalytic efficiencies similar to previously documented Gram negative bacterial MurE ligases. We discuss how
38 these data accord with the conservation of active site residues common to DL-DAP-incorporating bacterial MurE ligases
39 and of the probability of a horizontal gene transfer event within the plant peptidoglycan pathway.

40

41 **Introduction**

42 The endosymbiotic theory for the origin of photosynthetic eukaryotes proposes that an engulfed cyanobacterium evolved
43 into the first ancestors of chloroplasts (Dagan et al., 2013; Ponce-Toledo et al., 2017). As with bacteria, these organelles
44 (cyanelles) were surrounded by a peptidoglycan (or murein) wall (Scott et al., 1984). In bacteria, peptidoglycan covers
45 the organism in a mesh-like ‘sacculus’ conferring resistance to osmotic stress, and a species-specific shape and size.
46 Although originally considered likely that peptidoglycan was lost from all photosynthetic organelles immediately after
47 the glaucophyte branch (Pfanzagl et al., 1996), there has been an accumulation of evidence including sensitivity of
48 chloroplast division to peptidoglycan-directed antibiotics, fluorescent labelling studies and gene knockout phenotypes to
49 indicate that many streptophytes, including the charophyte algae (Matsumoto et al., 2012; Takano et al., 2018) and some
50 bryophytes and pteridophytes (sister lineages to seed plants) (Takano and Takechi, 2010; Hirano et al., 2016), may have
51 chloroplasts that synthesize peptidoglycan. Furthermore, in gymnosperms (Lin et al., 2017) and also a diverse number of
52 eudicots (van Baren et al., 2016) all the critical genes for peptidoglycan synthesis have been identified, although a
53 potential penicillin binding protein (PBP) typically required for peptidoglycan cross-linking has not been confirmed in
54 eudicots.

55 The earliest evidence for peptidoglycan in embryophytes was uncovered when antibiotics affecting bacterial
56 peptidoglycan synthesis in the bryophyte moss *P. patens* (Kasten and Reski, 1997; Katayama et al., 2003) and lycophytes
57 and ferns (Izumi et al., 2008) were found to cause a decrease in chloroplast number with the formation of giant
58 (macro)chloroplasts. Subsequently, genomics and *in silico* analyses confirmed the presence of all essential bacterial genes

59 for peptidoglycan biosynthesis (Rensing et al., 2008). These genes are nuclear-encoded, predominantly plastid-targeted
60 (Machida et al., 2006; Homi et al., 2009) and transcribed, as revealed by expressed sequence tags (ESTs). More recently,
61 a peptidoglycan layer surrounding *P. patens* chloroplasts has been visualized using a fluorescently labelled substrate
62 (Hirano et al., 2016) and electron microscopy (Sato et al., 2017).

63 Peptidoglycan in Gram negative bacteria has a repeating disaccharide backbone of β -(1,4) linked N-acetylglucosamine
64 (GlcNAc) and N-acetylmuramic acid (MurNAc) to which is appended a stem peptide comprising L-Ala, D-Glu, D,L-
65 DAP, D-Ala--D-Ala. Variations in the amino acid residues have been identified and are consequent on either the
66 specificity of the Mur ligases (MurC-F) or later modifications in peptidoglycan biosynthesis. In Gram positive bacteria
67 MurE typically incorporates L-Lys as opposed to D,L-DAP, although Bacilli are a notable exception and several other
68 amino acids have been identified in this position (Schleifer and Kandler, 1972; Barreteau et al., 2008; Vollmer et al.,
69 2008). The stem peptides of adjacent saccharide strands are crosslinked by transpeptidation to stabilize the mature
70 peptidoglycan (see biosynthetic pathway Figure 1).

71 Knock-out of *P. patens* homologs of bacterial peptidoglycan synthesis genes *Ddl*, *MurA*, *MurE*, *MraY*, *MurJ* or *PBP1A*,
72 results in a macrochloroplast phenotype, similar in appearance to antibiotic treatments that target their gene products,
73 while complementation with the intact genes restores the wild type number of about 50 typical chloroplasts per cell
74 (Machida et al., 2006; Homi et al., 2009; Hirano et al., 2016; Takahashi et al., 2016; Utsunomiya et al., 2020). Cross-
75 species complementation using a *P.patens MurE* (*PpMurE*) knockout showed that *Anabaena MurE* (*AnMurE*) fused to
76 the plastid-targeting signal of *PpMurE* can also restore the wild type chloroplast phenotype (Garcia et al., 2008). In
77 contrast, the homologous *Arabidopsis thaliana* gene, *AtMurE*, failed to complement the *PpMurE* mutant (Garcia et al.,
78 2008). Interestingly, *MurE* knockouts in both *A. thaliana* and *Zea mays*, appear bleached as opposed to having a
79 macrochloroplast phenotype, are deficient in chloroplast thylakoids and lack many plastid RNA polymerase-regulated
80 chloroplast transcripts, indicating that angiosperm MurE has a primary function in plastid gene expression and biogenesis
81 rather than plastid division *per se* (Garcia et al., 2008; Williams-Carrier et al., 2014).

82 Although data suggestive of the formation of chloroplast peptidoglycan is available, no direct observation of the
83 peptidoglycan precursors or the operation of the chloroplast peptidoglycan synthetic pathway has yet been made.
84 Therefore, here, using pathway-inhibiting antibiotics to drive the accumulation of peptidoglycan intermediates, we
85 establish that in a basal land plant, *P. patens*, the six *Mur* genes and *Ddl* actively synthesize all the main precursors of the
86 peptide stem of peptidoglycan. Furthermore, we show that the pentapeptide building blocks are identical to those of most
87 typical Gram negative bacteria, including the cyanobacteria, plus the Chlamydiae, the ‘acid fast’ *Mycobacterium* spp. and
88 some Gram positive bacilli, where D,L-DAP is incorporated instead of L-Lys. Consistent with and supportive of this

89 observation, we show that *in vitro* the moss MurE ligase, PpMurE, incorporates D,L-DAP in strict preference to L-Lys as
90 the third amino acid within the stem peptide, as would be consistent with the cyanobacterial ancestral origin of the
91 chloroplast, and the enzyme kinetics of PpMurE are similar to cyanobacterial and other Gram negative D,L-DAP-
92 incorporating MurE ligases.

93 **Materials and Methods**

94 **Plant Material**

95 *P. patens* (Gransden strain, GrD13) was grown on modified KNOPS medium with 5 mM diammonium tartrate, to
96 promote chloronemata formation (Schween et al., 2003). The medium was solidified with 0.85 % (w/v) plant agar
97 (Sigma) and overlaid with 9 cm cellophane discs (AA Packaging). Plants were grown in 90 mm diameter x 20 mm vented
98 tissue culture dishes sealed with Micropore (3M) surgical tape in a plant growth room at 21°C under continuous light
99 from Sylvania white F100W tubes at 65-100 $\mu\text{mol}\cdot\text{m}^{-2}\cdot\text{s}^{-1}$. After being homogenised axenically in water in a 250 ml flask
100 using an IKA T18 digital Ultra Turrax homogeniser, for one to two 12 s bursts, *P. patens* protonemata were cultured as 2
101 ml aliquots per 25 ml solid KNOPS plus tartrate.

102 **Confocal Microscopy of Antibiotic Treated *P. patens* Protonemata**

103 Confocal single plane images and Z-series stacks were acquired on a Leica SP5 microscope, using a 63 x 1.4 Oil UV
104 immersion objective with the 405 nm and 496 nm laser lines and transmitted light, and photo multiplier tube spectral
105 detection adjusted for the chlorophyll emission (735-790 nm). Images were processed using the Fiji distribution
106 of ImageJ v2.0.0.

107 **Trichloroacetic Acid (TCA) Extraction of Plant Metabolites**

108 Antibiotics were added to KNOPS plus tartrate agar at 100 $\mu\text{g ml}^{-1}$ carbenicillin, 100 $\mu\text{g ml}^{-1}$ D-cycloserine or 200 $\mu\text{g ml}^{-1}$
109 phosphomycin. After 15 days tissue was harvested, weighed and ground in liquid nitrogen using a pestle and mortar
110 before being frozen at -80°C. To extract TCA-soluble plant metabolites the tissue was ground again in 5 ml g^{-1} of ice cold
111 10% (w/v) TCA (Fisons AR grade) before being mixed gently in 50 ml Falcon tubes on a rolling shaker for 30 min at 4°C
112 (Roten et al., 1991). Insoluble material was pelleted at 48,000 $\times\text{g}$, 10 min, 2°C, the supernatant was retained and the pellet
113 reextracted twice more, first with 2.5 $\text{ml}\cdot\text{g}^{-1}$ and then with 1.25 $\text{ml}\cdot\text{g}^{-1}$ (of the original pellet weight) of ice cold 10%
114 (w/v) TCA. The pooled supernatants were extracted into an equal volume of diethyl ether, to remove TCA, by manually
115 shaking for 3 x 20 s in a separating funnel before recovering the lower, aqueous layer. The ether extraction of the aqueous
116 phase was repeated twice more. The pH of the combined lower phases was restored to pH 7-8 using 1 M NaOH and
117 residual ether was removed *in vacuo* at which point, the sample was lyophilised.

118 **Purification of Muropeptide Precursors**

119 The nucleotide precursors in the TCA-soluble metabolite extracts were first partially purified by size exclusion using a
120 Superdex Peptide 10/300GL column. The freeze-dried pellets were resuspended in deionised water, applied to the column
121 as a 500 µl aliquot, eluted with deionised water and collected as 0.5 ml fractions at 0.5 ml min⁻¹. The likely elution
122 volume of molecules of interest was established by elution of 20 nmols UDP-MurNAc-DAP-pentapeptide and 20 nmols
123 UDP-*N*-acetyl-glucosamine (Sigma) standards.

124 The A₂₆₀ of pooled Superdex Peptide fractions of 1-2 ml was used to determine the upper limit of the total concentration of
125 UDP species and an estimated 2, 10 or 20 nmols UDP species in 2 ml 10 mM ammonium acetate, pH 7.5, was loaded
126 onto a MonoQ 50/5 GL column equilibrated in the same buffer. Bound molecules were eluted with a 27 ml linear gradient
127 of 10 mM to 0.81M ammonium acetate (pH 7.5), at 0.7 ml.min⁻¹ and collected as 1ml fractions using an Äkta Pure where
128 the eluate absorbance was recorded at A₂₃₀, A₂₅₄ and A₂₈₀. Peaks with an absorbance ratio of usually 1:2 A₂₈₀:A₂₅₄ were
129 selected for freeze drying and mass spectrometry.

130 **Mass Spectrometric Nano-spray Time of Flight Analysis of Peptidoglycan UDP-MurNAc Precursors**

131 Identity of UDP-MurNAc precursors were confirmed by negative ion time of flight mass spectrometry using a Waters
132 Synapt G2Si quadrupole-time of flight instrument operating in resolution mode, equipped with a nanospray source
133 calibrated with an error of less than 1 ppm with sodium iodide over a 200-2500 m/z range (Catherwood et al.,
134 2020). Samples, freeze dried three times to remove ammonium acetate, were diluted in LCMS grade 50% v/v
135 acetonitrile to between 1 µM and 5 µM. They were introduced into the instrument using Waters thin wall nanoflow
136 capillaries and up to 20 minutes of continuum data were collected at a capillary voltage of 2.0 kV, cone and source
137 offset voltages of 100 V and a source offset of 41 V, respectively. Source and desolvation temperatures were 80°C
138 and 150°C respectively, desolvation and purge gas flow rates were both 400 l.min⁻¹. Scan time was 1 s with an
139 interscan time of 0.014 s. Scans were combined into centred mass spectra by Waters Mass Lynx software. Resolution
140 (m/z/half-height spectral peak width) was measured as 1 in 20,100.

141 **Construction of Heterologous Expression Plasmids**

142 *PpMurE* (derived from Pp3c23_15810V3.2) and *AnMurE* (derived from *Anabaena* sp. strain PCC 7120 *MurE*
143 WP_010995832.1 Q8YWF0|MURE_NOSS1) were inserted into the vector pPROEX HTa (Addgene) in order to be
144 expressed in frame with an amino terminal, TEV protease-cleavable, hexa-histidine (His6) tag. The *MurE* sequences were
145 PCR amplified from their respective cDNAs (Machida et al., 2006; Garcia et al., 2008) in pTFH22.4 using the primers
146 *PpMurE_L63_Forward* (TTTGCACATGTTGAAAATGGGGTTTGGGGATTCGAAATTGACGGATCG) and
147 *PpMurE_Reverse* (AAACGCGCGCCGCTTATTTTCTAAGTCGCAAAGCCTCCCGACATTCCTC) and
148 *Anabaena_PCC7120_MurE_Forward*

149 (TTTGCGGGTCTCTCATGAAATTGCGGGAATTACTAGCGACAGTAGACAGTG) and
150 *Anabaena_PCC7120_MurE_Reverse*
151 (AAACGCGCGGCCGCTTATAATTTTTCTTTCTGTCAAAGCGGCGGTGCG). The amplified region for
152 *PpMurE* started at leucine 63, effectively deleting the chloroplast transit peptide at the cleavage site predicted by the
153 ChloroP1.1 Prediction server (Emanuelsson, 1999) and introducing a unique *NcoI*-compatible *PciI* site around the novel
154 ATG and a *NotI* site immediately 3' to the stop codon. A TAA stop codon was substituted for the native TGA. The
155 *AnMurE* primers amplified the cDNA and novel *BsaI* and *NotI* sites were introduced 5' and 3' to the ATG start and TAA
156 stop codons, respectively. The former was sited to create a *NcoI*-compatible 5' cohesive end. The vector pPROEX HTa
157 was restricted with *NcoI* and *NotI* and gel purified before being ligated to *PciI*-*NotI* restricted *PpMurE_L63* or *BsaI*-
158 *NotI* restricted *AnMurE* PCR fragments that had been cleaned up with a PCR clean up kit (Qiagen). Coding sequences
159 were confirmed by Sanger sequencing (Eurofins).

160 **Expression of *PpMurE_L63* and *AnMurE* and Protein Purification**

161 For protein purification *Escherichia coli* strains were tested for optimal expression: BL21 DE3 (ThermoFisher) was
162 selected for *PpMurE_L63_pPROEX* and BL21(DE3), with the chaperone plasmid pG-KJE8 (Takara Bio Inc.), was
163 selected for *AnMurE_pPROEX*. These were grown in L-Broth plus 0.2% v/v glucose, 100 $\mu\text{g ml}^{-1}$ ampicillin and 35 μg
164 ml^{-1} chloramphenicol at 37°C to an A_{600} of 0.6 when *PpMurE* protein expression was induced with 0.5 mM IPTG and
165 *AnMurE* expression was induced by 0.5 mM IPTG with 1.5 $\text{mg}\cdot\text{ml}^{-1}$ arabinose and 8 $\text{ng}\cdot\text{ml}^{-1}$ tetracycline to induce pG-
166 KJE8 chaperones. Over-expressing cells were then grown overnight at 19°C. Bacteria were harvested by centrifugation at
167 5600 x g, 15 min at 4°C and resuspended in Buffer A: 50 mM HEPES-NaOH, 0.5 M NaCl, 10 mM imidazole and 10%
168 v/v glycerol (pH 7.5) containing EDTA-free protease inhibitor tablets, as recommended by the supplier (Pierce), and 2.5
169 mg ml^{-1} lysozyme, with gentle mixing for 30 min at 4°C. Lysis was by sonication on ice for 10 x 15 s bursts at 70%,
170 interspersed by 1-2 min cooling on ice. Insoluble material was pelleted at 50,000 xg for 30 min at 4°C and the supernatant
171 loaded directly onto a 5 ml His Trap HP (GE Healthcare) at 2 $\text{ml}\cdot\text{min}^{-1}$ and washed with 50 ml Buffer A at 4 $\text{ml}\cdot\text{min}^{-1}$ at
172 4°C. Bound material was eluted with an 100 ml linear gradient to 100% Buffer B: 50 mM HEPES-NaOH, 0.5 M NaCl,
173 5% w/w glycerol and 0.5 M imidazole (pH 7.5) at 4 $\text{ml}\cdot\text{min}^{-1}$. Selected peak fractions were pooled and concentrated in
174 either 30 or 50 kDa MWCO Vivaspin concentrators (GE Healthcare), for *AnMurE* or *PpMurE_L63*, respectively, at
175 2,800 xg at 4°C. Proteins were further purified by size exclusion chromatography on Superdex G200 XK26 (GE Life
176 Sciences) pre-equilibrated and eluted with 50 mM HEPES-NaOH, 150 mM NaCl (pH 7.5) and purity of the eluted MurE
177 proteins was established by SDS-PAGE (Supplemental Figure S3). Pooled peak fractions were dialysed against DB2: 30

178 mM HEPES-NaOH, 1 mM MgCl₂, 50 mM NaCl, 50% v/v glycerol with 0.2 mM PMSF, 1 μM leupeptin, 1 μM pepstatin,
179 3 mM dithiothreitol (pH 7.6) overnight at 4°C, before storage at -20°C and -80°C.

180 **TEV Protease-Cleaved Protein Preparation**

181 Bacteria were expressed as above, harvested and lysed using a cell disruptor and the proteins first purified on 5ml His
182 Trap HP columns, using Buffer A and B (pH 8.0) as above, except that 100 mM Tris replaced 50 mM HEPES and Buffer
183 A included 2% v/v glycerol, 10 mg.l⁻¹ DNase1 (DN25) and 1 mM DTT. Pooled fractions were exchanged into a buffer of
184 50 mM PIPES, 100 mM NH₄SO₄, 200 mM KCl, 20 mM MgCl₂, 1 mM DTT, 30 mM imidazole, 2% v/v glycerol (pH
185 7.7), using a stack of four 5ml HiTrap Desalting columns (Pharmacia). Peak fractions were incubated for 48h at 4°C in
186 the ratio 1 mg TEV protease: 50 mg protein before reverse His-tag purification, collecting the column flow through.
187 Samples were concentrated using 50 kDa concentrators as above.

188 *Streptococcus pneumoniae* MurE and *Pseudomonas aeruginosa* MurF were over-expressed and purified exactly as
189 described (Blewett et al., 2004; Majce et al., 2013).

190 **Mur Ligase Activity Assays**

191 The assays employed a continuous spectrophotometric method following ATP consumption at 37°C in a Cary 100
192 UV/Vis double beam spectrophotometer. Mur ligase catalysed ADP release, coupled to NADH oxidation by pyruvate
193 kinase and lactate dehydrogenase, led to stoichiometric consumption of NADH measured by a fall in the A₃₄₀. Assay
194 volumes were 0.2 ml and contained 50 mM PIPES, 10 mM MgCl₂ adjusted to pH 6.7 for AnMurE or 50 mM Tricine, 10
195 mM MgCl₂ adjusted to pH 8.7 for PpMurE_L63, 1 mM dithiothreitol, 0.2 mM NADH, 2 mM phosphoenol pyruvate,
196 1mM ATP, 50 mM.min⁻¹ pyruvate kinase and 50 mM.min⁻¹ lactate dehydrogenase (as assayed by the manufacturer,
197 Sigma). Ligases were diluted prior to assay as required in 50 mM HEPES pH 7.7, 50 mM KCl, 1 mM MgCl₂, 3 mM
198 DTT, 50% v/v glycerol, 0.2 mM PMSF. Concentrations of UDP-MurNAc dipeptide, Mur ligase and amino acid
199 substrates were as described in the text or table legends. Control rates were collected usually in the absence of the amino
200 acid, or UDP-MurNAc-dipeptide as specified, and the activity of the enzyme was initiated by addition of the missing
201 component. Mur ligase initial rates were recorded as mols ADP.mol Mur ligase⁻¹.s⁻¹ (ADP/s) within the linear range of
202 the time course of the assay.

203

204

205 **Results**

206 **Identification of antibiotics with the most profound effect on *P. patens* chloroplast division**

207 *P. patens* was grown on a variety of antibiotics that impact peptidoglycan biosynthesis in bacteria in order to select those
208 best able to cause an accumulation of peptidoglycan intermediates in the moss, so that they might be more readily
209 detected. Of the antibiotics tested the three that appeared most specific at inhibiting peptidoglycan synthesis, as measured
210 by a widespread macrochloroplast phenotype with least effect on chlorophyll intensity, were phosphomycin (500 $\mu\text{g}\cdot\text{ml}^{-1}$)
211 ¹), a PEP analog that inhibits MurA by alkylating an active site cysteine residue (Figure 1¹), the β -lactam ampicillin (100
212 $\mu\text{g}\cdot\text{ml}^{-1}$), which binds covalently to the active site serine of PBPs (Figure 1⁷), and D-cycloserine (20 $\mu\text{g}\cdot\text{ml}^{-1}$), with at least
213 two enzyme targets in peptidoglycan biosynthesis, DDL (Figure 1²) and alanine racemase (Figure 2 B, D and G) . Even at
214 higher concentrations, where growth rate was impaired, the protonemata were green indicating chlorophyll synthesis and
215 therefore chloroplast function was not significantly impaired. The impact of antibiotics that had either a more profound
216 and pleiotropic effect or that had little impact on phenotype are described in Supplemental Text S1 and include
217 vancomycin, bacitracin, murgocil and A22 (Figure 2 C, E, F and H).

218 **The TCA-extracted metabolome contains peptidoglycan precursors in *P. patens***

219 *P. patens* was grown separately on the three most specific and effective antibiotics, phosphomycin (400 $\mu\text{g}\cdot\text{ml}^{-1}$), D-
220 cycloserine (100 $\mu\text{g}\cdot\text{ml}^{-1}$), and carbenicillin (100 $\mu\text{g}\cdot\text{ml}^{-1}$) to facilitate accumulation of different peptidoglycan precursor
221 molecules (Figure 1^{1, 2 and 7}). After size exclusion and anion exchange chromatography to purify UDP-linked
222 intermediates from the TCA-extracted metabolome, mass spectrophotometric analysis identified precursors common to
223 most Gram negative bacterial cell wall syntheses (Table 1 and Figure 3 C, identified precursors numbered 1-5). Precursor
224 molecules were detected only in the earlier fractions from the Superdex Peptide column (Figure 3 B), as expected from
225 the elution profiles of UDP-GlcNAc and UDPMurNAc-pentapeptide standards (not shown).

226 The identification of UDP-MurNAc-Ala-Glu-D,L-DAP in three of the samples as well as the D,L-DAP pentapeptide
227 (Table 1 and Figure 3 C, numbers 4 and 5), together with the inability to identify UDP-MurNAc-Ala-Glu-Lys or UDP-
228 MurNAc-Lys-pentapeptide suggested that *in vivo*, PpMurE specifically incorporated DL-DAP in the third position of
229 stem peptide. By comparison, when the plant was grown on phosphomycin (Figure 1¹), anticipated to block synthesis of
230 UDP-MurNAc, only the UDP-GlcNAc precursor was identified (Table 1 and Figure 3 C, number 1). Interestingly, this
231 metabolite was not detected in the samples treated with the other antibiotics.

232 Similarly, the MurC and D products, UDP-MurNAc-Ala and UDP-MurNAc-Ala-Glu were detected in the D-cycloserine-
233 grown extract consistent with the accumulation of precursors up to the UDP-MurNAc-tripeptide MurF substrate (Figure 3
234 C, numbers 2 and 3). From the MonoQ anion exchange chromatograms (Figure 3, C) and the mass spectral data

235 (Supplemental Figure S2) we can conclude that use of the different antibiotics proved to be an effective way to ensure
236 most of the intermediates were detected, confirming the utility of this method for the purpose.

237 ***P. patens* MurE incorporates DL-DAP into the peptidoglycan stem peptide**

238 To account for the composition of the *P.patens* peptidoglycan stem peptide, we analysed the activity and substrate
239 specificity of the MurE ligase protein product of its *murE* gene, with the predicted 62 residue chloroplast transit peptide
240 sequence deleted (PpMurE_L63). The enzyme was compared with the cyanobacterial *Anabaena* MurE ligase. Analysis of
241 the ability of both AnMurE and PpMurE_L63 to utilise D,L-DAP D,D-DAP L,L-DAP and L-Lys revealed that both
242 MurE enzymes were catalytically active in the aminoacylation of UDP-MurNAc-dipeptide, Removal of the His tag by
243 TEV protease cleavage did not enhance the efficiency of either enzyme (Figure 4, B and Supplemental Figure S4) and
244 significantly, both proteins favoured D,L-DAP as a substrate over the other DAP diastereoisomers (Figure 4, A).
245 Noticeable was the slow rate of turnover of D,D-DAP by PpMurE_L63, in particular, possibly indicative of a weak
246 stereo-selectivity for the L- over the D stereocentre of DAP utilised by the enzyme when at high concentrations.
247 Significantly, neither enzyme incorporated L-Lys. As a control, lysylation of UDP-MurNAc-Ala-Glu was also assayed
248 with the L-Lys specific *Streptococcus pneumoniae* Pn16 MurE (Blewett et al., 2004) and resulted in a rate (v_0) of 1.94
249 ADP.s⁻¹ at 150 μM L-Lys, with the same UDP-MurNAc-dipeptide and ATP concentrations as the other assays (data not
250 shown).

251 That the assay followed the aminoacylation of UDP-MurNAc-dipeptide by D,L-DAP to yield D,L-DAP tripeptide was
252 confirmed by the ability of the assay product to be utilised as a substrate by *Pseudomonas aeruginosa* MurF (PaMurF).
253 This was achieved in the same coupled assay by adding PaMurF at t=0, initiating the MurE ligase reaction with D,L-DAP
254 and then the MurF ligase with D-Ala-D-Ala as the second substrate once the MurE reaction had reached completion to
255 yield the UDP-MurNAc-pentapeptide (Supplemental Figure S5).

256 **pH and Temperature Optima of *P. patens* and *Anabaena* MurE**

257 Prior to kinetic investigation of the properties of PpMurE the pH optimum was determined, with that of the
258 cyanobacterial AnMurE, by comparing rate of ADP generated (v_0) at pH 5.7-9.7 at approximately saturating
259 concentrations of its substrates (Supplemental Figure S6, A-D). Neither of the coupled enzymes in the MurE/ADP release
260 assay was a major factor affecting rate over the pH range studied as evidenced by the independence of the measured
261 MurE rate from coupling enzyme concentration. Additionally, the similarity of activities of the MurE proteins in
262 different buffers allowed us to discount the impact of buffers over the pH range under consideration (Supplemental Figure
263 S6, B and D). Assuming saturation with substrates and the only variable responsible for a change in enzyme activity was
264 pH range we fitted v_0 data vs pH to an equation that follows the relationship of activity *versus* pH. From these data it was

265 concluded that the optimum for AnMurE is 7.5 and that for PpMurE_L63 is approximately pH 7.5-8.5. The data fit for for
266 PpMurE_L63 ($R^2 = 0.94$ and 0.89 , for 1 and 2 x coupling enzymes, respectively) is better than that for AnMurE ($R^2 =$
267 0.78) indicating that the assumption that other variables (kinetic constants and substrate ionization) are not influenced by
268 pH may be less true for AnMurE.

269 ***P. patens* MurE has similar kinetic properties to cyanobacterial MurE**

270 The two enzymes AnMurE and PpMurE_L63 were assayed to calculate their kinetic efficiency for the preferred substrate
271 D,L-DAP. From the tabulated data PpMurE_L63 was more sensitive to substrate inhibition from D,L-DAP than AnMurE,
272 as indicated by its greater R^2 value for fit of data to the kinetics of substrate inhibition compared to those for standard
273 Michaelis Menten kinetics (Figure 4, B and the two fitted curves in Supplemental Figure S4, C and D). However, the
274 K_{cat}^{APP}/K_M^{APP} ratio for the plant enzyme were similar to the cyanobacterial one, the most marked difference being the lower
275 D,L-DAP K_M^{APP} value, indicative that the plant enzyme may operate at lower substrate concentrations *in vivo*. These
276 figures were compared with reported data for other MurE activities (Supplemental Figure S7) and reveal that the plant
277 and cyanobacterial MurE are at least as catalytically active, as indicated by the K_{cat}^{APP}/K_M^{APP} ratio, as the bacterial
278 homologs. It was apparent that removal of the His tag by TEV protease cleavage did not enhance the efficiency of either
279 enzyme (Figure 4, B and Supplemental Figure S4, B and D).

280 **Conservation of amino acid residues common to DL-DAP-incorporating MurE ligases**

281 BLASTP searches and ClustalW (EMBL-EBI) alignment indicated that the closest bacterial homolog to PpMurE is the
282 MurE of *Gemmatomonidates bacterium* (50.0% homology), which is a photoheterotrophic Gram negative bacterium in a
283 phylum quite distal to the cyanobacteria (Zeng et al., 2014). The next closest is the Gram positive *Bacillus fortis* (43.0%),
284 which would be anticipated to incorporate D,L-DAP (Barreteau et al., 2008). Both are considerably more closely related
285 than the cyanobacterial AnMurE (37.8%), determined in this paper to be D,L-DAP incorporating, *E.coli* MurE^{D,L-DAP}
286 (34.9%) and *Mycobacterium tuberculosis* MurE^{D,L-DAP} (34.7%). The L-Lys incorporating enzymes, all from Gram
287 negative species, share still less homology: *Thermatoga maritima* MurE^{L-Lys} (33.0%), *Streptococcus pneumoniae* MurE
288 (30.1%) and *Staphylococcus aureus* MurE^{L-Lys} (26.6%). Likewise, the neighbour-joining phylogram computed in Jalview
289 (Supplemental Figure S8) placed AnMurE as more distantly related than *Gemmatimonadetes* to plant MurE, as
290 represented by PpMurE and the algal streptophytes *Mesotaenium endlicherianum* MurE and *Coleochaete scutata* MurE.
291 *M. endlicherianum* (66.2%) represents a late charophyte ancestor within the Zygnemophyceae which are predicted to be
292 on a branch point preceding embryophyte evolution (Donoghue and Paps, 2020), whereas MurE from *Klebsormidium*
293 *nitens* (41.8%) and *C. scutata* (51.3%) in the Klebsomidiophyceae and Coleochaetaceae, respectively, and also within
294 the charophyte algae, are on more divergent branches.

295 To relate homology to functionality, PpMurE was aligned in Clustal Omega (EMBL-EBI) with homologs of both L-Lys-
296 and DL-DAP-incorporating MurE ligases (Supplemental Figure S9). Many amino acid residues are conserved not only
297 between MurE from bacterial and early plant species but also across the Mur ligase family (as indicated by asterisks on
298 Supplemental Figure S9). Mur ligases comprise three domains: an N-terminal Rossmann-fold domain responsible for
299 binding the UDP-MurNAc substrate; a central ATP-binding domain and a C-terminal domain associated with binding the
300 incoming amino acid. Most of the amino acids conserved between the different Mur ligases lie within the central ATP-
301 binding domain, those in the N- and C-termini generally do not co-localise with the known substrate binding residues.
302 Amino acids of published importance for ATP binding (species abbreviation subscripted); the P-loop within
303 TGTXGKT^{Sa}, E220^{Mt}, D356^{Sa}, N347^{Mt}, R377^{Mt} and R392^{Mt} are conserved in the plant enzymes *M. endlicherianum* MurE
304 and PpMurE, as well as a lysine, K219^{Sa}, carbamylated in MurD for positioning the MgATP complex for the generation
305 of a transient UDP-MurNAc-phosphodi-peptide intermediate (Dementin et al., 2001). K360^{Sa} and Y343^{Mt} have undergone
306 conservative changes. Similarly, residues that bind UDP-MurNAc, S28^{Ec}, HQA45^{Ec}, NTT158^{Ec}, E198^{Mt}, S184^{Ec},
307 QXR192^{Ec} and H248^{Mt} are no less conserved in plants than they are between bacteria.
308 Although most of the UDP-MurNAc-tripeptide interactions are within the MurE central domain, those made in relation to
309 the appended amino acid, D,L-DAP or L-Lys, are within the C-terminal domain. All of the identified bacterial MurE
310 residues that interact with D,L-DAP are highly conserved in plant MurE proteins. More specifically, with reference to *E.*
311 *coli* MurE and *M. tuberculosis* MurE, it is possible to distinguish those that interact with either the D- or L-stereocentre
312 carboxylates of D,L-DAP : G464^{Ec}, E468^{Ec}, D413^{Ec} and N414^{Ec}, which bond to the D-stereocentre, R389^{Ec}, which bonds
313 with the L-stereocentre, and especially R416^{Ec}, which interacts with both the L- and D-centre carboxylates. Of these
314 R389^{Ec}, N414^{Ec}, R416^{Ec}, G464^{Ec} and E468^{Ec} are less consistently present in MurE ligases from Gram positive bacteria
315 that incorporate L-Lys, a decarboxylated derivative of D,L-DAP, which has only been reported to interact with the
316 R383^{Sa}, D406^{Sa} and E460^{Sa} residues (Ruane et al., 2013). Similarly, the pattern of charged residues in the C-terminal
317 domain of the basal streptophyte MurE (those highlighted red or purple in Supplemental Figure S9) would indicate a
318 binding cleft for the amino acid substrate that is more basic and resembles that of the Gram negative MurE ligases.
319 Together these data are in complete accord with our kinetic findings that D,L-DAP is the preferred substrate in plants and
320 AnMurE, rather than L-Lys. As would be anticipated from the phylogeny, the more closely related *G. bacterium* MurE
321 aligns strongly with the Gram negative DL-DAP incorporating enzymes, and includes the DNPR motif, which confers
322 specificity for the D-stereocentre carboxyl and amino groups of D,L-DAP, indicating that this phylum is most likely to
323 incorporate DL-DAP.
324

325 Discussion

326 *P. patens* peptidoglycan is synthesized from a UDP-MurNAc-D,L-DAP-pentapeptide

327 Growth of *P. patens* on the antibiotics phosphomycin, D-cycloserine and ampicillin facilitated the detection, by mass
328 spectrophotometric analysis of the TCA-extracted metabolome, of peptidoglycan intermediates up to UDP-MurNAc-Ala-
329 Glu-DAP-Ala-Ala in the moss. These data enable us to conclude that the identical basic building blocks for the Gram
330 negative bacterial cell wall are found in basal embryophytes. With evidence for knock-out phenotypes for *P. patens*
331 homologs of bacterial *MraY*, *MurJ* and *PBP1A* and the presence of mRNA for *MurG* (Machida et al., 2006; Homi et al.,
332 2009; Utsunomiya et al., 2020) it would be expected that the D,L-DAP-containing pentapeptide within the stroma is lipid-
333 linked then flipped across the chloroplast inner envelope membrane and polymerised into peptidoglycan to form a
334 ‘sacculus’ bounding the organelle, as indicated from fluorescent-labelling using a D-Ala-D-Ala analogue (Hirano et al.,
335 2016). By analogy with bacteria and from the predicted transit peptides of the peptidoglycan-maturing proteins it is
336 anticipated that the peptidoglycan will lie between the inner and outer membranes of the chloroplast, although this has yet
337 to be determined (Figure 1).

338 PpMurE appends D,L-DAP to UDPMurNAc-Ala-Glu

339 From our data, it is evident that the moss MurE ligase, with the transit peptide omitted, PpMurE_L63, can efficiently
340 append D,L-DAP to UDP-MurNAc-L-Ala-D-Glu *in vitro*, as can the cyanobacterial enzyme from *Anabaena* sp. strain
341 PCC 7120, AnMurE. This is in accordance with the D,L-DAP content of peptidoglycan in the cyanobacteria
342 *Synechococcus* sp. and *Synechocystis* sp. (Jurgens et al., 1983; Woitzik, 1988) and is inconsistent with the observation
343 that *Anabaena cylindrica* may incorporate L-Lys (Hoiczyk and Hansel, 2000). Our *in vitro* MurE enzymological data also
344 complement the mass spectrometric analysis of the antibiotic-grown *P. patens* which identified UDP-MurNAc-D,L-DAP
345 intermediates as being present *in vivo* in the TCA-extracted metabolome.

346 That UDP-MurNAc-L-Ala-D-Glu is an efficient substrate for PpMurE_L63 is significant in that there is no obvious
347 homolog in most green plants for glutamate racemase (MurI), exceptions include the glaucophyte alga *Cyanophora*
348 *paradoxa* (Contig25539), the charophyte alga *K. nitens* (GAQ85716.1) but not *M. endlicherianum*, a zygenematophycean
349 alga proposed to be closest to the embryophyte branch point. Here, this function may be replaced by a D-alanine amino
350 transferase (DAAA), of which there are two genes having weak homology to *Bacillus subtilis* DAAA in both *P. patens*
351 and *M. endlicherianum* (Phytozome v.13 *P. patens*: Pp3c6_5420 (15.7%), Pp3c16_17790 (14.7%) and OneKP *M.*
352 *endlicherianum*: WDCW scaffolds 2009723 (17.6%) and 2007189 (16.5%)). Alternatively *P. patens* diaminopimelate
353 epimerase (DapF), like Chlamydial DapF, may possess the dual specificity required to racemase L-Glu to D-Glu in
354 addition to its epimerization of L,L-DAP to D,L-DAP (De Benedetti et al., 2014).

355 **Substrate Preference of AnMurE and PpMurE**

356 The high degree of specificity of both AnMurE and PpMurE_L63 for D,L-DAP, over the alternatives L,L-DAP, D,D-
357 DAP and L-Lys, is consistent with other D,L-DAP-incorporating enzymes assayed *in vitro*, including *E. coli* MurE, *M.*
358 *tuberculosis* MurE and *Chlamydia trachomatis* MurE, for which L-Lys is either a very poor substrate or is not accepted
359 at all (Supplemental Table S7). Similarly, the L-Lys-incorporating *S. aureus* MurE does not incorporate D,L-DAP *in*
360 *vitro*. Not all MurE ligases are as selective, *Thermotoga maritima* MurE incorporates L-Lys and D-Lys in almost equal
361 amounts *in vivo* (Huber, 1986) and can efficiently incorporate D,L-DAP *in vitro* (Boniface et al., 2006). In this regard it is
362 notable that *T. maritima* MurE possesses a DDPR motif, which includes the arginine residue of the consensus DNPR of
363 D,L-DAP-incorporating enzymes which hydrogen bonds to and stabilises D,L-DAP, consequently the almost complete
364 absence of D,L-DAP in *T. maritima* peptidoglycan has been attributed to its low intracellular concentration. This almost
365 absolute specificity of most MurE ligases is indicative of a requirement that the stem peptide be composed of the correct
366 amino acids to facilitate optimal transpeptidation (Vollmer et al., 2008).

367 **PpMurE is a slow but efficient MurE ligase**

368 Kinetic analyses of PpMurE_L63 demonstrated an enzymatic efficiency similar to bacterial MurE homologs, as estimated
369 by comparison of K_{cat}^{APP}/K_M^{APP} (Supplemental Table S7). Further comparisons with other D,L-DAP-incorporating
370 enzymes, and in particular those of the obligate intracellular pathogens *C. trachomatis* and *M. tuberculosis*, revealed the
371 plant MurE to have a similarly low K_M for the amino acid substrate relative to the L-Lys-incorporating enzymes. This
372 may reflect either (or both) a lower abundance of D,L-DAP or the potential toxicity of the D,L-diamino acid, particularly
373 in a eucaryotic cell (Kolukisaoglu and Suarez, 2017). A higher K_M for L-Lys-incorporating MurE ligases has been
374 attributed to the much greater abundance of this amino acid in bacteria (Mengin-Lecreux et al., 1982; Ruane et al., 2013).
375 The availability of the D,L-DAP substrate in plants, as in cyanobacteria and Chlamydiae, is not in question as the
376 biosynthesis of L-Lys is catalysed by DAP decarboxylase (LysA) from D,L-DAP which is ultimately derived from
377 aspartate (Hudson et al., 2006).

378 Comparison of the PpMurE_L63 K_{cat}^{APP} with the bacterial enzymes reveals the rate of turnover to be quite low, possibly
379 reflecting the apparent low density of peptidoglycan surrounding the chloroplast and a concomitant slower rate of
380 synthesis compared to rapidly dividing, free-living bacteria. Moreover, the plant enzyme has UDP-MurNAc-Ala-Glu
381 kinetics best fitted to a substrate inhibition model, possibly to ensure that peptidoglycan synthesis proceeds at a rate
382 insufficient to consume the majority of available prenyl phosphates that are otherwise required for other pathways.

383 It is important to mention that the *P. patens* genome encodes two MurE homologs (PpMurE1: Pp3c23_15810, studied in
384 this paper, and PpMurE2: Pp3c24_18820) which have 72.2% amino acid identity to each other over the conventional

385 bacterial MurE ligase domains and 48.4% identity overall. PpMurE2 primarily differs from PpMurE1 in encoding a long,
386 relatively unstructured extension at the amino terminus and a short carboxy terminal extension (expanded description in
387 Supplemental Figure S10). Although the DNPR motif and other amino acids associated with D,L-DAP binding are
388 retained in PpMurE2, knock out mutations of PpMurE1 alone results in a comprehensive macrochloroplast phenotype
389 (Machida et al., 2006; Garcia et al., 2008), consistent with the hypothesis that this protein is sufficient for peptidoglycan
390 synthesis in the moss. Moreover, preliminary *in vitro* experiments indicate that intact PpMurE2 does not function as a
391 MurE ligase (data not shown) and we would suggest that both the amino and carboxy terminal extensions have been
392 acquired during streptophyte evolution to participate in novel interactions thereby facilitating an alternative function for
393 MurE within the chloroplast transcription and translation apparatus.

394 In contrast to *P. patens* (and the Polypodiidae ferns, Supplemental Figure S10), many in the same and closely related
395 phylla encode a single *MurE* homolog with both the amino and carboxy terminal extensions and aligning more closely to
396 PpMurE2, yet these proteins would be anticipated to function as MurE ligases. We propose the shorter MurE in *P. patens*
397 and the Polypodiidae ferns represents a de-evolution of streptophyte MurE to more closely resemble its bacterial
398 counterpart. It has yet to be determined at what point in streptophyte evolution the function of MurE changed and whether
399 in any plants it remains a bifunctional protein capable of both MurE ligase activity and interaction with chloroplast RNA
400 polymerase in chloroplast transcription.

401 That basal embryophyte MurE has evolved a new role essential to plastid photomorphogenesis in seed plants indicates an
402 exaptation from its original function in peptidoglycan biosynthesis and plastid division (Williams-Carrier et al., 2014).
403 This raises the intriguing question why important residues of the D,L-DAP-binding motif are retained, in similar
404 proximity to the ATPase domain, in these proteins. We would speculate that the novel function of the MurE-like proteins
405 in seed plants could have evolved consequent on the two whole gene duplication events which occurred in an ancestral
406 moss, as opposed to in the liverworts or hornworts (Lang et al., 2018).

407 **Predicted streptophyte peptidoglycan structure from peptidoglycan gene homologies**

408 The moss ‘sacculus’, like that of Chlamydiae, has been recalcitrant not only to visualisation by electron microscopy but
409 also to common extraction protocols, making analysis of the mature polymer a future goal. The moss chloroplast
410 envelope membranes were found to be closely appended with little dense intervening material (Takano and Takechi,
411 2010; Matsumoto et al., 2012; Sato et al., 2017), likewise in Chlamydiae the apparent deficit of a bounding sacculus lead
412 to the term the ‘chlamydial anomaly’ (Packiam et al., 2015). This is in marked contrast to most cyanobacteria where the
413 cell wall is highly cross-linked and forms a broad, electron dense layer (Hoiczyk and Hansel, 2000). Intermediate
414 between these extremes is the earliest side branch in plant evolution, the glaucophyte algae, where the cyanelles comprise

415 a peptidoglycan layer that has been more tractable to visualisation and analysis (Pfanzagl et al., 1996; Higuchi et al.,
416 2016).

417 It would appear that progressive transition of a bacterium from free-living to endosymbiont or pathogen and thence to an
418 integrated organelle is associated with a reduction in substance of the sacculus. Presumably there are not the same
419 osmotic constraints and risks of dehydration within the host cell and the vestigial peptidoglycan may function primarily
420 or exclusively for the purpose of assembly of the division apparatus. Additionally, it may be that for cyanobacterial
421 evolution into a cyanelle and subsequently a plastid that a finer, net-like cell wall would be a prerequisite if extensive
422 exchange of larger molecules, including lipids and proteins, were to occur. Supportive of this suggestion is the fact that
423 most of the bacterial PBPs which cross-link the lipid-linked GlcNAc-MurNAc-pentapeptide precursor, have been
424 identified as having no predicted product from RNA-seq data (data not shown). Currently the only reported exception is a
425 PBP1A homolog, the transpeptidase and transglycosylase functions of which have an almost complete knock out
426 phenotype (Machida et al., 2006; Takahashi et al., 2016).

427 We also propose that streptophyte peptidoglycan must differ in its mature form by being uniquely modified to distinguish
428 it from the peptidoglycan of potential plant pathogens. The *P. patens* genome encodes a battery of proteins that include
429 peptidoglycan-binding and LysM domains and which frequently but not invariably include cell export signals (data not
430 shown). Many of these proteins will be part of the defences of the plant cell which are activated on detection of fungal
431 and bacterial cell wall material. To evade the host cell defences it is anticipated that an endosymbiont, obligate pathogen
432 or evolving organelle must protect its peptidoglycan from the host defences, conceivably by modification of the peptide
433 stem (Wolfert et al., 2007) or the GlcNAc-MurNAc backbone (Davis and Weiser, 2011). Predictions as to what those
434 modifications might be in streptophytes are hampered by the fact that the ancestry of the modifying enzymes is not
435 necessarily cyanobacterial. We have reported here the closer homology of PpMurE to MurE in the Gemmatimonadetes
436 phylum and we can further include *P. patens* PBP1A, MurF, MurD, MurG and Ddl as most closely related to homologs
437 within the same Fibrobacteres-Chlorobi-Bacteroidetes group of Gram negative bacteria (data not shown). The diverse
438 origins of several peptidoglycan biosynthesis-related proteins have previously been reported (Sato and Takano, 2017).
439 Therefore, it appears highly probable that a horizontal gene transfer event of a distinct Gram negative peptidoglycan-
440 related gene cluster must have occurred early in the plant lineage. Hence we conjecture a simultaneous transfer of
441 peptidoglycan-modifying genes could have occurred that would introduce novel modifications to the mature polymer,
442 distinct from any in cyanobacteria. This is not without precedent, as the divergent glaucophyte algae were found to
443 append *N*-acetyl-putrescine to the second residue in the stem peptide (Pfanzagl et al., 1996).

444 Here we have determined that chloroplast peptidoglycan in the streptophyte, *P. patens*, is constructed from typical Gram
445 negative UDP-MurNAc-D,L-DAP-pentapeptide peptidoglycan precursor. However, we propose that the final
446 polymerised structure derived from this building block differs from its cyanobacterial progenitor by being both less
447 highly polymerised and, to distinguish it from plant pathogens and thereby evade the plant immune response,
448 significantly modified.

449

450 **Supplemental Data**

451 Supplemental Text S1. Effects of antibiotics on *P. patens*

452 Supplemental Figure S2. Negative ion nanospray TOF mass spectra of TCA-extracted peptidoglycan intermediates

453 Supplemental Figure S3. PAGE gel of AnMurE and PpMurE_L63 after gel filtration

454 Supplemental Figure S4. D,L-DAP substrate curves for AnMurE and PpMurE_L63

455 Supplemental Figure S5. Assay data demonstrating PaMurF utilises the product of AnMurE and PpMurE_L63

456 Supplemental Text S6. Activities of AnMurE and PpMurE_L63 with pH and buffer

457 Supplemental Table S7. Comparison of AnMurE and PpMurE_L63 kinetics with published data for other MurE ligases

458 Supplemental Figure S8. Neighbour joining phylogram of MurE of Gram-negative bacteria and early plant species

459 Supplemental Figure S9. Clustal Omega multiple sequence alignment of MurE homologs

460 Supplemental Figure S10. Phylogram of evolutionary relationship of both PpMurE proteins to selected MurE homologs

461

462 **Acknowledgements**

463 The authors thank Professor Hiroyoshi Takano (Kumamoto University, Japan) for kindly providing the pTFH22.4 vectors
464 with *Anabaena* (PCC7120 Q8YWF0|MURE_NOSS1) and *P. patens* (Pp3c23_15810V3.2) *MurE* cDNA and Dr Sven
465 Gould (Heinrich Heine University, Düsseldorf, Germany) for helpful discussion on chloroplast evolution. We are also
466 grateful to Julie Tod and Anita Catherwood (University of Warwick, UK) for synthesis of UDP-MurNAc-dipeptide, -
467 tripeptide and -pentapeptide and providing *Streptococcus pneumoniae* MurE and *Pseudomonas aeruginosa* MurF and Ian
468 Hands-Portman for access to and training in the School of Life Sciences Imaging Suite, University of Warwick, UK). We
469 also gratefully acknowledge Prof. Rebecca Goss (St Andrews, UK) for provision of pacidamycin.

470

471 **Barreteau H, Kovac A, Boniface A, Sova M, Gobec S, Blanot D (2008)** Cytoplasmic steps of
472 peptidoglycan biosynthesis. *FEMS Microbiol Rev* **32**: 168-207

473 **Blewett AM, Lloyd AJ, Echalié A, Fulop V, Dowson CG, Bugg TD, Roper DI (2004)**

474 Expression, purification, crystallization and preliminary characterization of uridine 5'-
475 diphospho-N-acetylmuramoyl L-alanyl-D-glutamate:lysine ligase (MurE) from
476 *Streptococcus pneumoniae* 110K/70. *Acta Crystallogr D Biol Crystallogr* **60**: 359-361

- 477 **Boniface A, Bouhss A, Mengin-Lecreulx D, Blanot D** (2006) The MurE synthetase from
478 *Thermotoga maritima* is endowed with an unusual D-lysine adding activity. *J Biol Chem*
479 **281**: 15680-15686
- 480 **Catherwood AC, Lloyd AJ, Tod JA, Chauhan S, Slade SE, Walkowiak GP, Galley NF, Puneekar**
481 **AS, Smart K, Rea D, Evans ND, Chappell MJ, Roper DI, Dowson CG** (2020) Substrate
482 and Stereochemical Control of Peptidoglycan Cross-Linking by Transpeptidation by
483 *Escherichia coli* PBP1B. *J Am Chem Soc* **142**: 5034-5048
- 484 **Dagan T, Roettger M, Stucken K, Landan G, Koch R, Major P, Gould SB, Goremykin VV,**
485 **Rippka R, Tandeau de Marsac N, Gugger M, Lockhart PJ, Allen JF, Brune I, Maus I,**
486 **Puhler A, Martin WF** (2013) Genomes of Stigonematalean cyanobacteria (subsection V)
487 and the evolution of oxygenic photosynthesis from prokaryotes to plastids. *Genome Biol*
488 **Evol** **5**: 31-44
- 489 **Davis KM, Weiser JN** (2011) Modifications to the peptidoglycan backbone help bacteria to
490 establish infection. *Infect Immun* **79**: 562-570
- 491 **De Benedetti S, Buhl H, Gaballah A, Klockner A, Otten C, Schneider T, Sahl HG,**
492 **Henrichfreise B** (2014) Characterization of serine hydroxymethyltransferase GlyA as a
493 potential source of D-alanine in *Chlamydia pneumoniae*. *Front Cell Infect Microbiol* **4**: 19
- 494 **Dementin S, Bouhss A, Auger G, Parquet C, Mengin-Lecreulx D, Dideberg O, van**
495 **Heijenoort J, Blanot D** (2001) Evidence of a functional requirement for a
496 carbamoylated lysine residue in MurD, MurE and MurF synthetases as established by
497 chemical rescue experiments. *Eur J Biochem* **268**: 5800-5807
- 498 **Donoghue P, Paps J** (2020) Plant Evolution: Assembling Land Plants. *Curr Biol* **30**: R81-R83
- 499 **Emanuelsson O, Nielsen, H., von Heijne, G.** (1999) ChloroP. *Protein Science* **8**: 978-984
- 500 **Garcia M, Myouga F, Takechi K, Sato H, Nabeshima K, Nagata N, Takio S, Shinozaki K,**
501 **Takano H** (2008) An Arabidopsis homolog of the bacterial peptidoglycan synthesis
502 enzyme MurE has an essential role in chloroplast development. *Plant J* **53**: 924-934
- 503 **Higuchi H, Takechi K, Takano H** (2016) Visualization of Cyanelle Peptidoglycan in
504 *Cyanophora paradoxa* Using a Metabolic Labeling Method with Click Chemistry.
505 *Cytologia* **81**: 357-358
- 506 **Hirano T, Tanidokoro K, Shimizu Y, Kawarabayasi Y, Ohshima T, Sato M, Tadano S,**
507 **Ishikawa H, Takio S, Takechi K, Takano H** (2016) Moss Chloroplasts Are Surrounded
508 by a Peptidoglycan Wall Containing D-Amino Acids. *Plant Cell* **28**: 1521-1532
- 509 **Hoiczyk E, Hansel A** (2000) Cyanobacterial cell walls: news from an unusual prokaryotic
510 envelope. *J Bacteriol* **182**: 1191-1199
- 511 **Homi S, Takechi K, Tanidokoro K, Sato H, Takio S, Takano H** (2009) The peptidoglycan
512 biosynthesis genes MurA and MraY are related to chloroplast division in the moss
513 *Physcomitrella patens*. *Plant Cell Physiol* **50**: 2047-2056
- 514 **Huber R, Langworthy, T. A., Konig, H., Thomm, M., Woese, C.R., Sleytr, U.B. and Stetter, K.**
515 **O.** (1986) *Thermotoga maritima* sp. nov. represents a new genus of unique extremely
516 thermophilic eubacteria *Arch. Microbiol.* **144**: 324-333
- 517 **Hudson AO, Singh BK, Leustek T, Gilvarg C** (2006) An LL-diaminopimelate aminotransferase
518 defines a novel variant of the lysine biosynthesis pathway in plants. *Plant Physiol* **140**:
519 292-301
- 520 **Izumi Y, Kuroki J, Nagafuji H, Lin X, Takano H** (2008) Effects of antibiotics that inhibit
521 bacterial peptidoglycan synthesis on plastid division in pteridophytes. *Cytologia* **73**:
522 393-400
- 523 **Jurgens UJ, Drews G, Weckesser J** (1983) Primary structure of the peptidoglycan from the
524 unicellular cyanobacterium *Synechocystis* sp. strain PCC 6714. *J Bacteriol* **154**: 471-478

- 525 **Kasten B, Reski R** (1997) β -Lactam antibiotics inhibit chloroplast division in a moss
526 (*Physcomitrella patens*) but not in tomato (*Lycopersicon esculentum*). *Journal of Plant*
527 *Physiology* **150**: 137-140
- 528 **Katayama N, Takano H, Sugiyama M, Takio S, Sakai A, Tanaka K, Kuroiwa H, Ono K** (2003)
529 Effects of antibiotics that inhibit the bacterial peptidoglycan synthesis pathway on moss
530 chloroplast division. *Plant Cell Physiol* **44**: 776-781
- 531 **Kolukisaoglu Ü, Suarez J** (2017) D-Amino Acids in Plants: New Insights and Aspects, but also
532 More Open Questions. *In* *Amino Acid - New Insights and Roles in Plant and Animal*,
533 **Lang D, Ullrich KK, Murat F, Fuchs J, Jenkins J, Haas FB, Piednoel M, Gundlach H, Van Bel**
534 **M, Meyberg R, Vives C, Morata J, Symeonidi A, Hiss M, Muchero W, Kamisugi Y,**
535 **Saleh O, Blanc G, Decker EL, van Gessel N, Grimwood J, Hayes RD, Graham SW,**
536 **Gunter LE, McDaniel SF, Hoernstein SNW, Larsson A, Li FW, Perroud PF, Phillips J,**
537 **Ranjan P, Rokshar DS, Rothfels CJ, Schneider L, Shu S, Stevenson DW, Thummler F,**
538 **Tillich M, Villarreal Aguilar JC, Widiez T, Wong GK, Wymore A, Zhang Y, Zimmer**
539 **AD, Quatrano RS, Mayer KFX, Goodstein D, Casacuberta JM, Vandepoele K, Reski R,**
540 **Cuming AC, Tuskan GA, Maumus F, Salse J, Schmutz J, Rensing SA** (2018) The
541 *Physcomitrella patens* chromosome-scale assembly reveals moss genome structure and
542 evolution. *Plant J* **93**: 515-533
- 543 **Lin X, Li N, Kudo H, Zhang Z, Li J, Wang L, Zhang W, Takechi K, Takano H** (2017) Genes
544 Sufficient for Synthesizing Peptidoglycan are Retained in Gymnosperm Genomes, and
545 *MurE* from *Larix gmelinii* can Rescue the Albino Phenotype of *Arabidopsis MurE*
546 Mutation. *Plant Cell Physiol* **58**: 587-597
- 547 **Machida M, Takechi K, Sato H, Chung SJ, Kuroiwa H, Takio S, Seki M, Shinozaki K, Fujita T,**
548 **Hasebe M, Takano H** (2006) Genes for the peptidoglycan synthesis pathway are
549 essential for chloroplast division in moss. *Proceedings of the National Academy of*
550 *Sciences* **103**: 6753-6758
- 551 **Majce V, Ruane KM, Gobec S, Roper DI** (2013) Crystallization and preliminary X-ray analysis
552 of a UDP-MurNAc-tripeptide D-alanyl-D-alanine-adding enzyme (PaMurF) from
553 *Pseudomonas aeruginosa*. *Acta Crystallogr Sect F Struct Biol Cryst Commun* **69**: 503-505
- 554 **Matsumoto H, Takechi K, Sato H, Takio S, Takano H** (2012) Treatment with antibiotics that
555 interfere with peptidoglycan biosynthesis inhibits chloroplast division in the desmid
556 *Closterium*. *PLoS One* **7**: e40734
- 557 **Mengin-Lecreulx D, Flouret B, van Heijenoort J** (1982) Cytoplasmic steps of peptidoglycan
558 synthesis in *Escherichia coli*. *J Bacteriol* **151**: 1109-1117
- 559 **Packiam M, Weinrick B, Jacobs WR, Jr., Maurelli AT** (2015) Structural characterization of
560 muropeptides from *Chlamydia trachomatis* peptidoglycan by mass spectrometry
561 resolves "chlamydial anomaly". *Proc Natl Acad Sci U S A* **112**: 11660-11665
- 562 **Pfanzagl B, Allmaier G, Schmid ER, A. DPM, Loffelhardt W** (1996) N-Acetylputrescine as a
563 Characteristic Constituent of Cyanelle Peptidoglycan in Glaucocystophyte Algae. *Journal*
564 *of Bacteriology* **178**: 6994-6997
- 565 **Ponce-Toledo RI, Deschamps P, Lopez-Garcia P, Zivanovic Y, Benzerara K, Moreira D**
566 (2017) An Early-Branching Freshwater Cyanobacterium at the Origin of Plastids. *Curr*
567 *Biol* **27**: 386-391
- 568 **Rensing SA, Lang D, Zimmer AD, Terry A, Salamov A, Shapiro H, Nishiyama T, Perroud PF,**
569 **Lindquist EA, Kamisugi Y, Tanahashi T, Sakakibara K, Fujita T, Oishi K, Shin IT,**
570 **Kuroki Y, Toyoda A, Suzuki Y, Hashimoto S, Yamaguchi K, Sugano S, Kohara Y,**
571 **Fujiyama A, Anterola A, Aoki S, Ashton N, Barbazuk WB, Barker E, Bennetzen JL,**
572 **Blankenship R, Cho SH, Dutcher SK, Estelle M, Fawcett JA, Gundlach H, Hanada K,**
573 **Heyl A, Hicks KA, Hughes J, Lohr M, Mayer K, Melkozernov A, Murata T, Nelson DR,**

- 574 **Pils B, Prigge M, Reiss B, Renner T, Rombauts S, Rushton PJ, Sanderfoot A, Schween**
575 **G, Shiu SH, Stueber K, Theodoulou FL, Tu H, Van de Peer Y, Verrier PJ, Waters E,**
576 **Wood A, Yang L, Cove D, Cuming AC, Hasebe M, Lucas S, Mishler BD, Reski R,**
577 **Grigoriev IV, Quatrano RS, Boore JL** (2008) The Physcomitrella genome reveals
578 evolutionary insights into the conquest of land by plants. *Science* **319**: 64-69
- 579 **Roten CA, Brandt C, Karamata D** (1991) Genes involved in meso-diaminopimelate synthesis
580 in *Bacillus subtilis*: identification of the gene encoding aspartokinase I. *J Gen Microbiol*
581 **137**: 951-962
- 582 **Ruane KM, Lloyd AJ, Fulop V, Dowson CG, Barreteau H, Boniface A, Dementin S, Blanot D,**
583 **Mengin-Lecreux D, Gobec S, Dessen A, Roper DI** (2013) Specificity determinants for
584 lysine incorporation in *Staphylococcus aureus* peptidoglycan as revealed by the
585 structure of a MurE enzyme ternary complex. *J Biol Chem* **288**: 33439-33448
- 586 **Sato N, Takano H** (2017) Diverse origins of enzymes involved in the biosynthesis of
587 chloroplast peptidoglycan. *J Plant Res* **130**: 635-645
- 588 **Sato N, Toyoshima M, Tajima N, Takechi K, Takano H** (2017) Single-Pixel Densitometry
589 Revealed the Presence of Peptidoglycan in the Intermembrane Space of the Moss
590 Chloroplast Envelope in Conventional Electron Micrographs. *Plant Cell Physiol* **58**:
591 1743-1751
- 592 **Schleifer KH, Kandler O** (1972) Peptidoglycan. Types of Bacterial Cell Walls and their
593 Taxonomic Implications. *Bacteriological Reviews* **36**: 407-477
- 594 **Schween G, Gorr G, Hohe A, Reski R** (2003) Unique Tissue-Specific Cell Cycle in
595 *Physcomitrella*. *Plant Biology* **5**: 50-58
- 596 **Scott OT, Castenholz RW, Bonnett HT** (1984) Evidence for a peptidoglycan envelope in the
597 cyanelles of *Glaucocystis nockii* Itzigsohn. *Arch Microbiol.* **139**: 130-138
- 598 **Takahashi Y, Takechi K, Takio S, Takano H** (2016) Both the transglycosylase and
599 transpeptidase functions in plastid penicillin-binding protein are essential for plastid
600 division in *Physcomitrella patens*. *Proc Jpn Acad Ser B Phys Biol Sci* **92**: 499-508
- 601 **Takano H, Takechi K** (2010) Plastid peptidoglycan. *Biochim Biophys Acta* **1800**: 144-151
- 602 **Takano H, Tsunefuka T, Takio S, Ishikawa H, Takechi K** (2018) Visualization of Plastid
603 Peptidoglycan in the Charophyte Alga *Klebsormidium nitens* Using a Metabolic Labeling
604 Method. *Cytologia* **83**: 375-380
- 605 **Utsunomiya H, Saiki N, Kadoguchi H, Fukudome M, Hashimoto S, Ueda M, Takechi K,**
606 **Takano H** (2020) Genes encoding lipid II flippase MurJ and peptidoglycan hydrolases
607 are required for chloroplast division in the moss *Physcomitrella patens*. *Plant Mol Biol*
- 608 **van Baren MJ, Bachy C, Reistetter EN, Purvine SO, Grimwood J, Sudek S, Yu H, Poirier C,**
609 **Deerinck TJ, Kuo A, Grigoriev IV, Wong CH, Smith RD, Callister SJ, Wei CL, Schmutz**
610 **J, Worden AZ** (2016) Evidence-based green algal genomics reveals marine diversity and
611 ancestral characteristics of land plants. *BMC Genomics* **17**: 267
- 612 **Vollmer W, Blanot D, de Pedro MA** (2008) Peptidoglycan structure and architecture. *FEMS*
613 *Microbiol Rev* **32**: 149-167
- 614 **Williams-Carrier R, Zoschke R, Belcher S, Pfalz J, Barkan A** (2014) A major role for the
615 plastid-encoded RNA polymerase complex in the expression of plastid transfer RNAs.
616 *Plant Physiol* **164**: 239-248
- 617 **Woitzik D, Weckesser, J. and Jurgens, U.J.** (1988) Isolation and Characterization of Cell Wall
618 Components of the unicellular cyanobacterium *synechococcus* sp PCC 6301. *J. Gen.*
619 *Microbiol.* **134**: 619-627
- 620 **Wolfert MA, Roychowdhury A, Boons GJ** (2007) Modification of the structure of
621 peptidoglycan is a strategy to avoid detection by nucleotide-binding oligomerization
622 domain protein 1. *Infect Immun* **75**: 706-713

623 **Zeng Y, Feng F, Medova H, Dean J, Koblizek M** (2014) Functional type 2 photosynthetic
624 reaction centers found in the rare bacterial phylum Gemmatimonadetes. Proc Natl Acad
625 Sci U S A **111**: 7795-7800
626
627

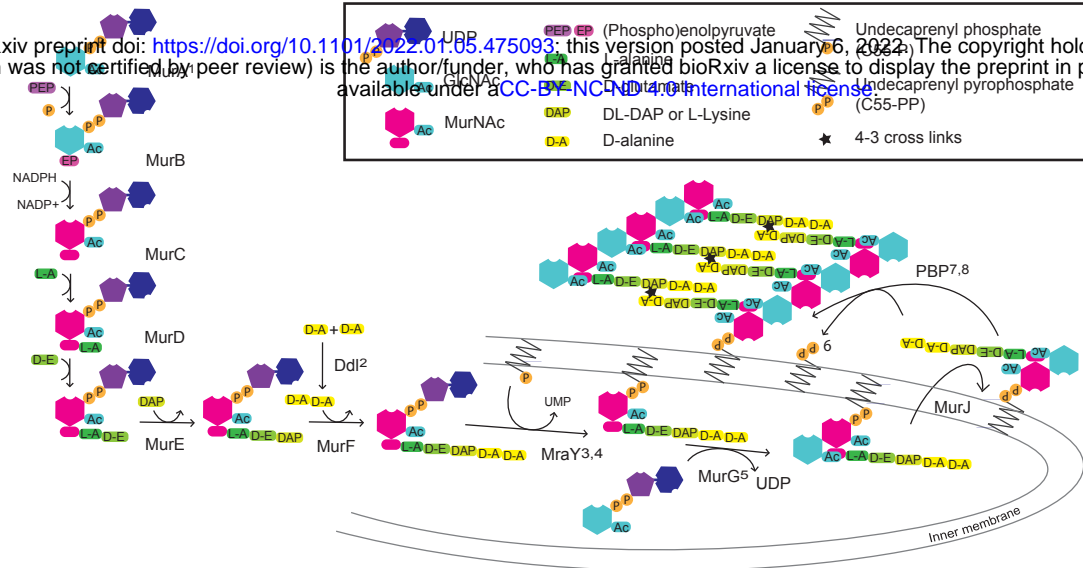


Figure 1 Schematic of the fundamental cytoplasmic and periplasmic enzyme steps in peptidoglycan (murein) biosynthesis. Enzymes: MurA-J, murein synthases A-J; Ddl, D-Ala--D-Ala ligase; MraY, phospho-N-acetylmuramoyl-pentapeptide-transferase and PBP, transglycosylase and transpeptidase activities of penicillin-binding proteins. Superscript numbers indicate targets for the following antibiotics: 1, phosphomycin, 2, D-cycloserine, 3, pacidamycin, 4, tunicamycin, 5, murgocil, 6, bacitracin, 7, penicillins and 8, vancomycin. The cytoplasmic Mur proteins MurA and MurB catalyze the formation of UDP-N-acetylmuramic acid (UDP-MurNAc), Mur ligases (MurC, D, E and F) sequentially append amino acids to form UDP-MurNAc-pentapeptide. The transmembrane protein MraY attaches MurNAc-pentapeptide to C55-P to yield C55-PP-MurNAc-pentapeptide (lipid I) and MurG GlcNAc transferase creates C55-PP-MurNAc-(pentapeptide)-GlcNAc (lipid II). Finally, the disaccharide pentapeptide monomer is flipped into the periplasm, polymerized by the transglycosylase activities of penicillin-binding-proteins (PBPs), or functionally related shape, elongation, division and sporulation (SEDS) proteins, and the peptides are 4-3 cross-linked to pre-existing peptidoglycan by the transpeptidase activities of PBPs or 3-3 cross-linked by L,D-transpeptidases. C55-PP is then subject to pyrophosphatase activity and C55-P recycled.

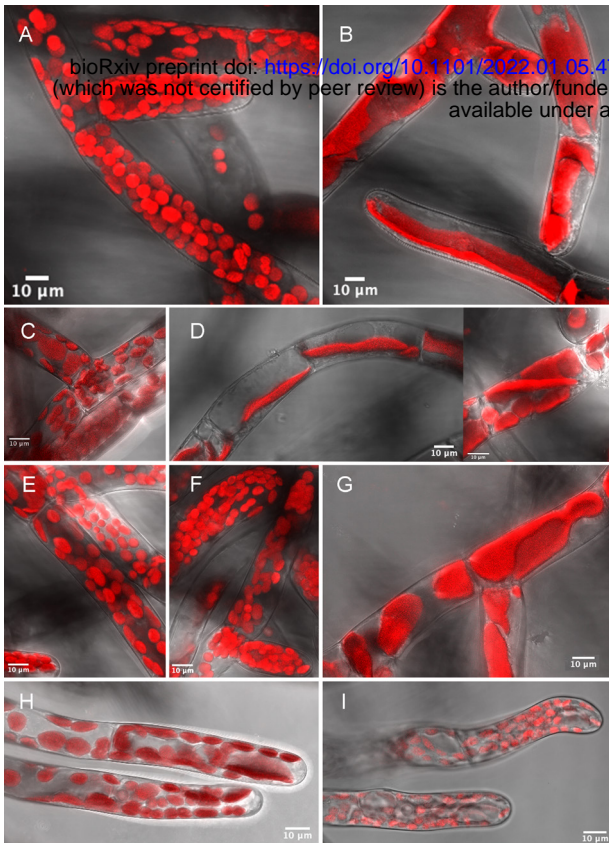


Figure 2 Confocal microscope images showing the effects of antibiotics on *P. patens* chloronemata. Chlorophyll autofluorescence (red) reveals macrochloroplasts consequent on growth on phosphomycin, D-cycloserine, vancomycin, bacitracin, ampicillin and A22. A. untreated, B. phosphomycin (500 $\mu\text{g.ml}^{-1}$), C. vancomycin (25 $\mu\text{g.ml}^{-1}$), D. D-cycloserine (20 $\mu\text{g.ml}^{-1}$, two images), E. bacitracin (100 $\mu\text{g.ml}^{-1}$), F. murgocil (10 $\mu\text{g.ml}^{-1}$), G. ampicillin (100 $\mu\text{g.ml}^{-1}$), H. A22 (2.5 $\mu\text{g.ml}^{-1}$) and I. A22 (10 $\mu\text{g.ml}^{-1}$). Sequential fluorescence and transmitted light images, from a Leica SP5 with 63 x oil immersion lens, were processed using LAS AF lite to optimise intensity and combined as hyperstacks using Fiji on Image J. Scale bars 10 μm .

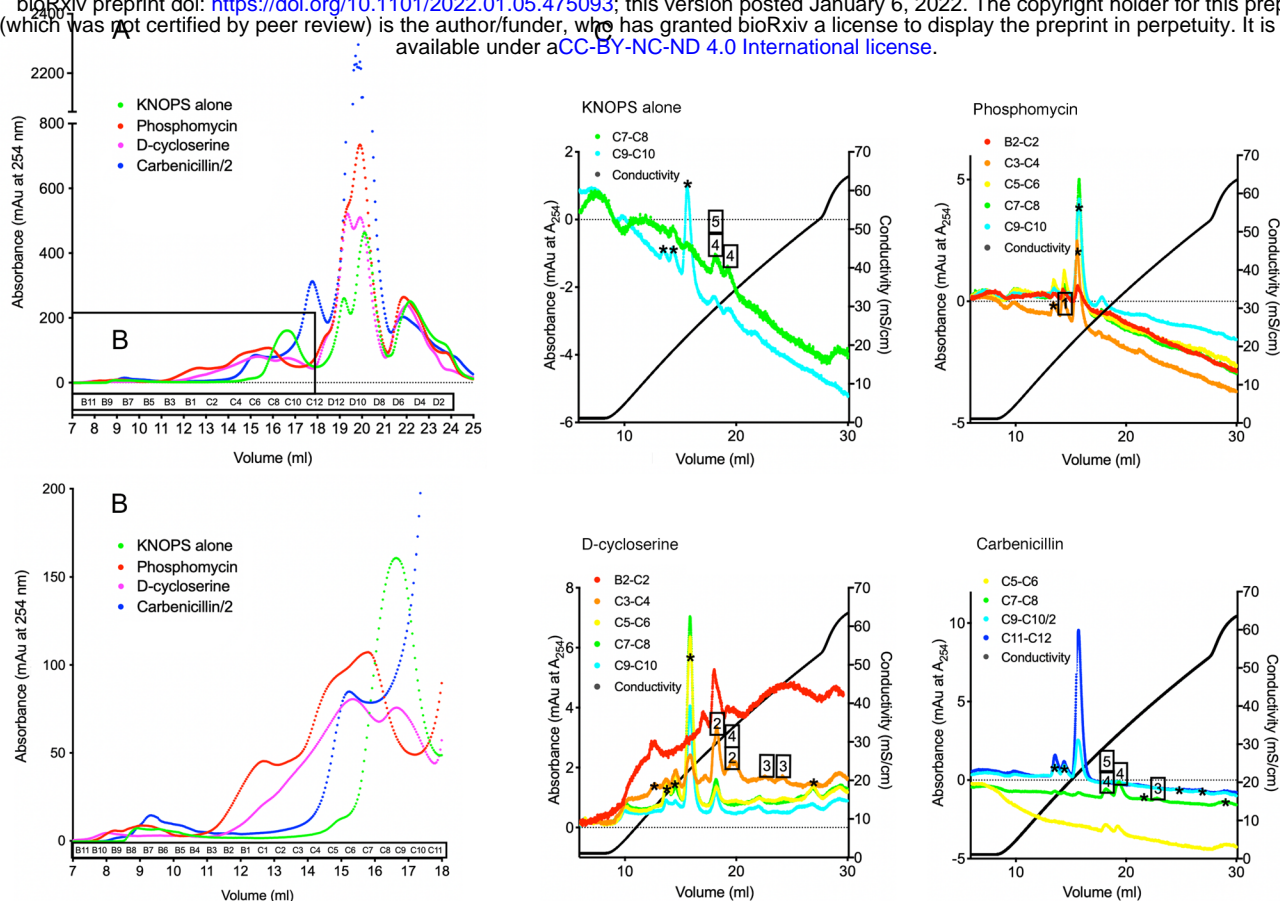


Figure 3 Size exclusion (Superdex Peptide, A and B) and ion exchange (MonoQ, C) chromatography elution profiles at A254 of the TCA-extracted metabolome from *P. patens* grown on KNOPS with and without antibiotics. A. Superdex Peptide traces for the four treatments; KNOPS alone, or KNOPS with phosphomycin ($400 \mu\text{g}\cdot\text{ml}^{-1}$), D-cycloserine ($100 \mu\text{g}\cdot\text{ml}^{-1}$) or carbenicillin ($100 \mu\text{g}\cdot\text{ml}^{-1}$). (For carbenicillin the A254 was divided by two). B. Enlargement of the earlier fractions, where the intermediates were anticipated to elute (as determined by controls). C. MonoQ traces of pooled Superdex Peptide fractions of 2-20 nmoles of UDP species (from B2-C12). Boxed numbers represent fractions positively identified as intermediates (see Table 1) and asterisks indicate peaks with no recognised component.

bioRxiv preprint doi: <https://doi.org/10.1101/2022.01.05.475093>; this version posted January 6, 2022. The copyright holder for this preprint (which was not certified by peer review) is the author/funder, who has granted bioRxiv a license to display the preprint in perpetuity. It is made available under aCC-BY-NC-ND 4.0 International license.

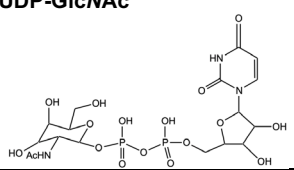
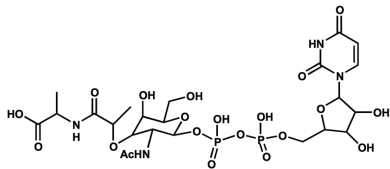
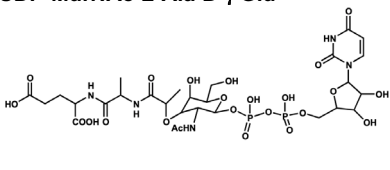
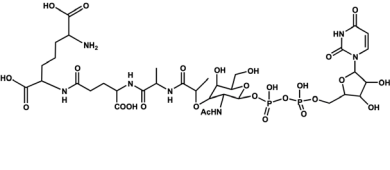
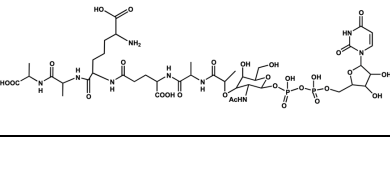
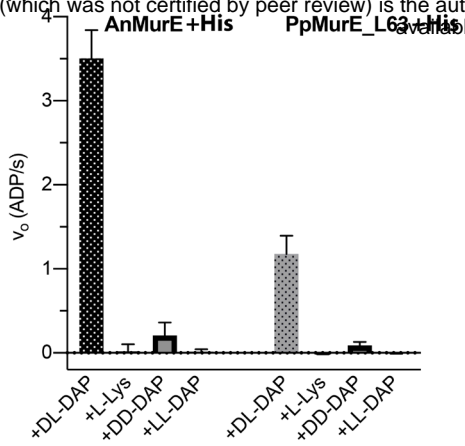
Peptidoglycan Intermediate	Number on MonoQ (Fig. 3)	Conductivity (µS/cm)	Growth Medium	Superdex Peptide and MonoQ Fractions	Species of Intermediate	Expected mZ	Nanospray TOF value consistent with expected
UDP-GlcNAc 	1	18.3	KNOPS + Phos ₄₀₀	C3-C4 F15	(m-1)/1	606.0738	606.0814
					(m+Na+1)/1	628.0557	628.0628
					(m-2)/2	302.5330	302.5352
UDP-MurNAc-L-Ala 	2	29.41 33.77	KNOPS + D-cyclo ₁₀₀	C3-C4 F19 C3-C4 F20	(m-2)/2	374.0621	374.0696 <i>374.0698</i>
					(m-1)/1	749.1320	749.1476 <i>749.1488</i>
					(m+Na+1)/1	771.1139	771.1294 <i>771.1281</i>
					(m+2Na+1)/1	793.0959	793.1107 <i>793.1127</i>
					(m+3Na+1)/1	815.0778	815.0909 <i>815.0963</i>
					(m+Na+2)/2	385.0531	385.0607 <i>385.0611</i>
UDP-MurNAc-L-Ala-D-γ Glu 	3	44.78 50.97	KNOPS + D-cyclo ₁₀₀	C3-C4 F23 C3-4 F24-25	(m-2)/2	438.5833	438.5928 <i>438.5935</i>
					(m+Na+2)/2	449.5744	449.5839 <i>449.5858</i>
					(m+2Na+2)/2	460.5653	460.5750 <i>460.5716</i>
	3	41.73	KNOPS + Cb ₁₀₀	C7-C8 F23	(m-2)/2	438.583	438.5916
					(m+Na+2)/2	449.5744	449.5829
					(m+2Na+2)/2	460.5653	460.5743
UDP-MurNAc-L-Ala-D-γ Glu-meso-DAP 	4	29.6 32.74	KNOPS alone	C7-C8 F18-19 C7-C8 F20	(m-2)/2	524.6258	524.6289 <i>524.6289</i>
					(m+Na+2)/2	535.6168	- <i>535.6196</i>
					(m+2Na+2)/2	546.6077	- <i>546.6108</i>
	4	33.77	KNOPS + D-cyclo ₁₀₀	C3-C4 F20	(m-2)/2	524.6258	524.6377
					(m+Na+2)/2	535.6168	535.6290
					(m+2Na+2)/2	546.6077	546.6197
					(m+3Na+2)/2	557.5987	557.6108
					(m-2)/2	524.6258	524.6317 <i>524.6324</i>
					(m+Na+2)/2	535.6168	535.6230 <i>535.6234</i>
					(m+2Na+2)/2	546.6077	546.6139 <i>546.6144</i>
4	29.68 32.83	KNOPS + Cb ₁₀₀	C7-C8 F19 C7-C8 F20	(m-2)/2	524.6258	524.6317 <i>524.6324</i>	
				(m+Na+2)/2	535.6168	535.6230 <i>535.6234</i>	
				(m+2Na+2)/2	546.6077	546.6139 <i>546.6144</i>	
5	29.6	KNOPS alone	C7-C8 F18-19	(m-2)/2	595.6629	595.6646	
				(m+Na+2)/2	606.6539	606.6553	
				(m-3)/3	396.7726	396.7740	
				(m-2)/2	595.6629	595.6693	
				(m+Na+2)/2	606.6539	606.6602	
				(m+2Na+2)/2	617.6446	617.6509	
				(m-3)/3	396.7726	396.7763	
UDP-MurNAc-L-Ala-D-γ Glu-meso-DAP-D-Ala 	5	29.6	KNOPS alone	C7-C8 F18-19	(m-2)/2	595.6629	595.6646
					(m+Na+2)/2	606.6539	606.6553
					(m-3)/3	396.7726	396.7740
	5	29.68	KNOPS + Cb ₁₀₀	C7-C8 F19	(m-2)/2	595.6629	595.6693
					(m+Na+2)/2	606.6539	606.6602
					(m+2Na+2)/2	617.6446	617.6509
					(m-3)/3	396.7726	396.7763

Table 1 UDP-linked intermediates in peptidoglycan biosynthesis as detected by mass spectrometry of the *P. patens* TCA-extracted metabolome, with expected mass:charge (mZ) ratios and actual TOF nanospray values as listed. (Figures in italics represent where a species was detected in more than one fraction). *P. patens* was grown on KNOPS medium with or without antibiotics, including Phos₄₀₀ (phosphomycin 400 µg.ml⁻¹), D-cyclo₁₀₀ (D-cycloserine 100 µg.ml⁻¹) and Cb₁₀₀ (carbenicillin 100 µg.ml⁻¹). Superdex Peptide (C) and MonoQ fractions (F) where the different species were identified are listed with their peak conductivities on MonoQ, as detailed in Figure 3. The negative ion nanospray TOF mass spectra from which the data are derived are in Supplemental Figure S2.



D,L-DAP	Michaelis Menten			Substrate Inhibition				<i>k_{cat}</i> / <i>K_M</i> <i>s⁻¹.mM⁻¹</i>
	<i>K_M</i> <i>μM</i>	<i>V_{max}</i> <i>s⁻¹</i>	<i>R</i> ²	<i>K_M</i> <i>μM</i>	<i>V_{max}</i> <i>s⁻¹</i>	<i>R</i> ²	<i>K_i</i> <i>μM</i>	
AnMurE+His	56.9	6.75	0.979	67.2	7.58	0.979	1480	119
AnMurE-His	39.4	4.34	0.988	39.4	4.34	0.988	3.06e ⁺¹²⁵	110
PpMurE_L63+His	8.16	1.79	0.903	15.2	2.41	0.950	340	220 159
PpMurE_L63-His	8.62	0.657	0.926	13.0	0.793	0.948	447	76.0 61.0

Figure 4 Substrate specificity and kinetics of AnMurE and PpMurE_L63. A, Activity of AnMurE and PpMurE_L63 with 150 μM D,L-DAP, L-Lys, D,D-DAP or L,L-DAP. Assays included 375 μM UDPMurNac-dipeptide and 100 or 300 nM AnMurE+His or PpMurE_L63+His in 50 mM Hepes pH 7.6, respectively. Results (v_o) are presented as ADP. s^{-1} (mols ADP.mol Mur ligase $^{-1}$. s^{-1}). Error bars are 95% confidence intervals of 5 or more rates from up to 8 replicate experiments. Students t test indicate D,D-DAP rates for both enzymes are significantly greater than those for either L,L-DAP or L-Lys. B. Michaelis Menten and substrate inhibition values for K_M (μM), V_{max} (ADP. s^{-1}) and R^2 (coefficient for data fit to either model), as computed by Prism, for both enzymes with and without His tags. All constants are 'apparent', obtained at fixed concentrations of the other two substrates. k_{cat} derives from V_{max} in mols ADP.mol Mur ligase $^{-1}$. s^{-1} . k_{cat}/K_M values are for Michaelis Menten kinetics for AnMurE and for substrate inhibition (bold) and Michaelis Menten kinetics (italics) for PpMurE_L63. (D,L-DAP substrate curves are in Supplemental Figure S4).

Supplemental Text S1 Effects of antibiotics on *P. patens*

bioRxiv preprint doi: <https://doi.org/10.1101/2022.01.05.475093>; this version posted January 6, 2022. The copyright holder for this preprint (which was not certified by peer review) is the author/funder, who has granted bioRxiv a license to display the preprint in perpetuity. It is made available under aCC-BY 4.0 International license.

Antibiotic D-threo-chloramphenicol (302.5 kDa) is a tetracycline antibiotic (200 and 100 µg.ml⁻¹), which complexes with C55-isoprenyl pyrophosphate, inhibiting recycling (Figure 1^{8,6} and Figure 2, C and E). Neither antibiotic typically traverse cytoplasmic membranes, and therefore a strong phenotype was not expected as it is anticipated they would have to penetrate not only the cytoplasmic membrane but also, potentially, the outer chloroplast membrane. It may be that any observed effect of these antibiotics was restricted to damaged or senescing cells. At high concentrations (500 µg.ml⁻¹) bacitracin did cause premature senescence.

A22 hydrochloride, a smaller molecule at 271.6 kDa, was tested at 2.5 and 10 µg.ml⁻¹ and was likewise found to result in macrochloroplast formation in some but not most cells, although at higher concentrations its impact was more pleiotropic and chloroplasts were considerably bleached (Figure 2, H and I). A22 inhibits MreB, an actin homolog and cytoskeletal protein that controls bacterial width in rod-shaped bacteria by spatiotemporal regulation of peptidoglycan synthesis. Since there is not an evident MreB homolog in the moss (Ozdemir et al., 2018), any effect of A22 may be consequent on a less specific effect on chloroplast heat shock proteins having homology to MreB, especially HSP70 (Gao and Gao, 2011).

Another antibiotic clearly pleiotropic in its effect was tunicamycin (0.2, 1.0 and 5.0 µg.ml⁻¹), a glycoprotein that inhibits the transfer of phospho-MurNAc-pentapeptide to the lipid carrier undecaprenyl pyrophosphate by *MraY* (Figure 1⁴). At concentrations equal to or above 1 µg.ml⁻¹ it caused chloroplast malformation, slow growth and apoptosis (data not shown). This could be attributed to its effect on the maturation of glycoproteins in the endoplasmic reticulum since, in eucaryotes, tunicamycin also blocks the transfer of UDP-GlcNAc to dolichol phosphate.

Pacidamycins 1 and 5, cationic peptides with homology to the bacteriophage ϕ X174 lysis protein Arg-Trp-x-x-Trp motif, believed to bind the cytoplasmic surface of *MraY* and thereby inhibiting it (Figure 1³) (Rodolis et al., 2014; Bugg and Kerr, 2019), had little effect on either growth rate or chloroplast division (data not shown). Likewise, Murgocil, a 448Da steroid-like molecule, which inhibits peptidoglycan synthesis in *Staphylococcus aureus* and is predicted to bind in the *MurG* active site blocking UDP-GlcNAc access (Figure 1⁵), when tested at 1, 5 and 25 µg.ml⁻¹ was found to have little effect on protonemata phenotype (Figure 2, F).

The effect of the three antibiotics, phosphomycin, D-cycloserine and ampicillin (Figure 3 B,D and G), subsequently selected for investigating the accumulation of peptidoglycan intermediates is detailed in the text of the paper.

Bugg TDH, Kerr RV (2019) Mechanism of action of nucleoside antibacterial natural product antibiotics. *J Antibiot* (Tokyo) 72: 865-876

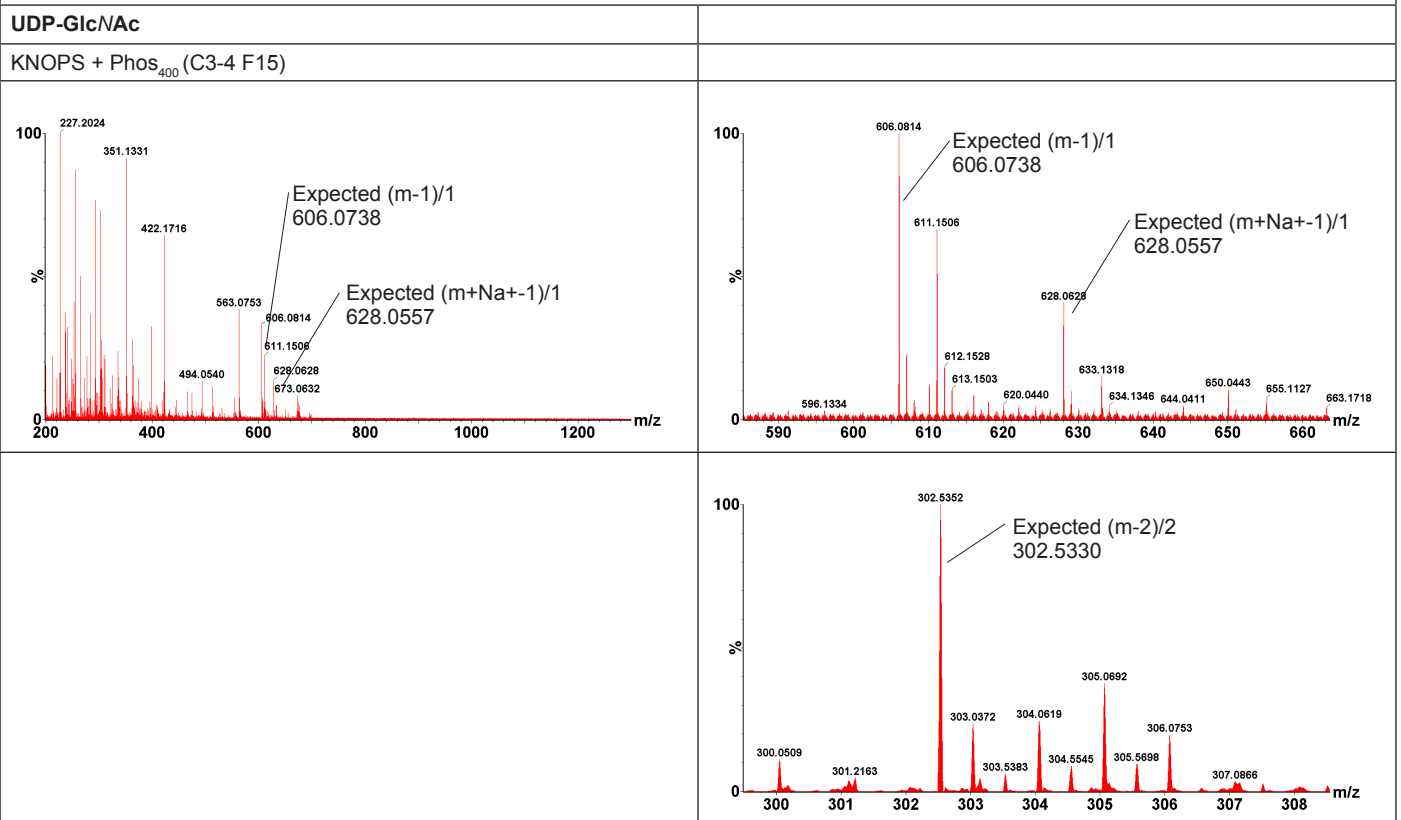
Gao H, Gao F (2011) Evolution of the chloroplast division machinery. *Frontiers in Biology* 6: 398-413

Ozdemir B, Asgharzadeh P, Birkhold AI, Mueller SJ, Rohle O, Reski R (2018) Cytological analysis and structural quantification of FtsZ1-2 and FtsZ2-1 network characteristics in *Physcomitrella patens*. *Sci Rep* 8: 11165

Rodolis MT, Mihalyi A, Ducho C, Eitel K, Gust B, Goss RJ, Bugg TD (2014) Mechanism of action of the uridyl peptide antibiotics: an unexpected link to a protein-protein interaction site in translocase *MraY*. *Chem Commun* (Camb) 50: 13023-13025

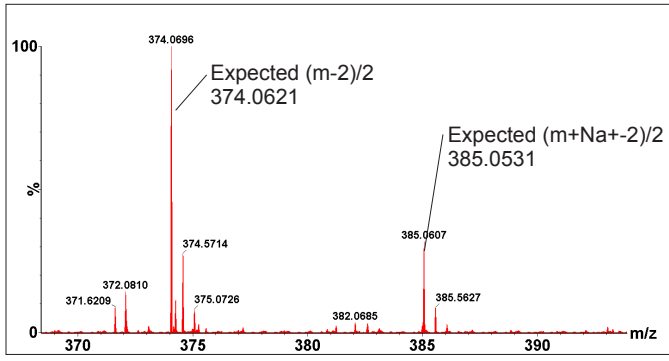
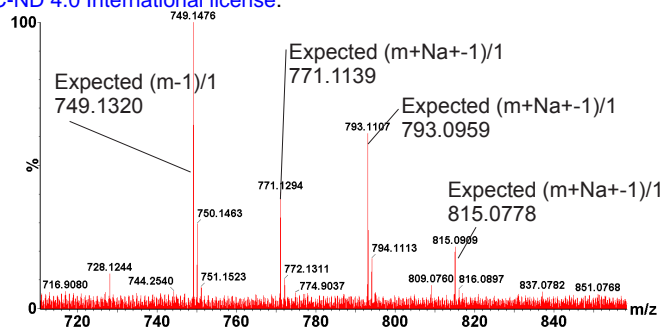
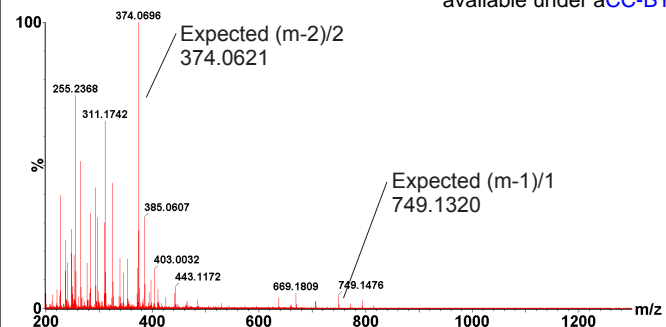
Supplemental Figure S2 Negative ion nanospray TOF mass spectra of TCA-extracted peptidoglycan intermediates, with the expected mass-to-charge (m/z) values for the different species. <https://doi.org/10.1101/2022.01.06.475099> was deposited on January 6, 2022. The copyright holder for this preprint (which was not certified by peer review) is the author/funder, who has granted bioRxiv a license to display the preprint in perpetuity. It is made available under aCC-BY-NC-ND 4.0 International license.

Phos₄₀₀ (phosphomycin 400 µg.ml⁻¹), D-cycloserine (D-cycloserine 100 µg.ml⁻¹) and C₂ (californicidin 100 µg.ml⁻¹). UDP-linked intermediates were purified by chromatography on Superdex Peptide and then MonoQ columns and their respective fractions (C and F) are indicated in brackets in the headers.

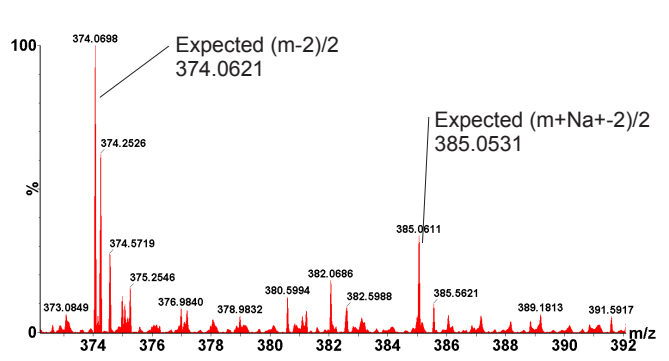
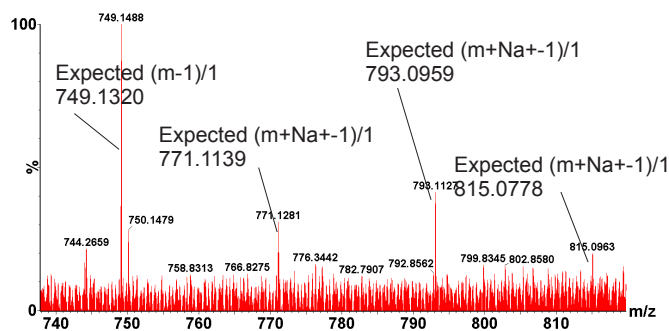
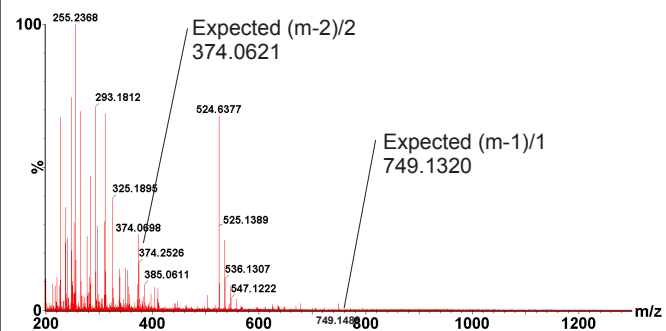


UDP-MurNAc-Ala

KNOPS + D-cycloserine₁₀₀ (C3-4 F19) <https://doi.org/10.1101/2022.01.05.475093>; this version posted January 6, 2022. The copyright holder for this preprint (which was not certified by peer review) is the author/funder, who has granted bioRxiv a license to display the preprint in perpetuity. It is made available under a [CC-BY-NC-ND 4.0 International license](https://creativecommons.org/licenses/by-nc-nd/4.0/).

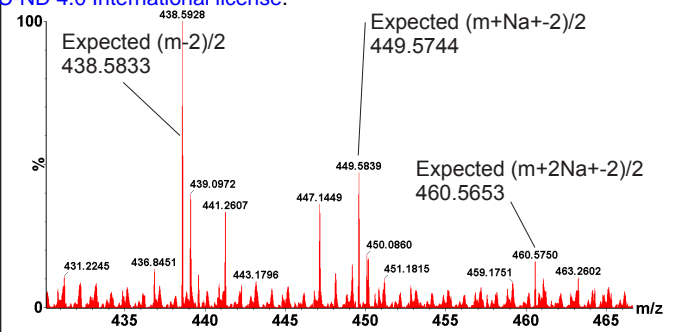
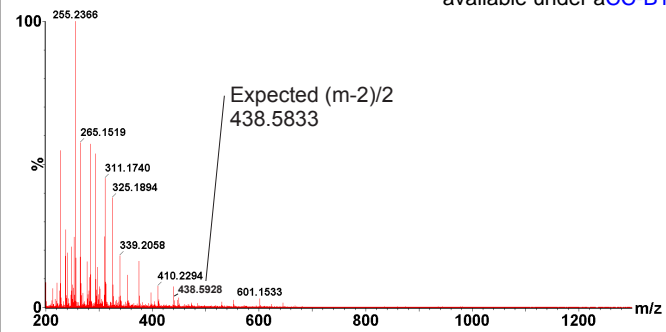


KNOPS + D-cycloserine₁₀₀ (C3-4 F20)

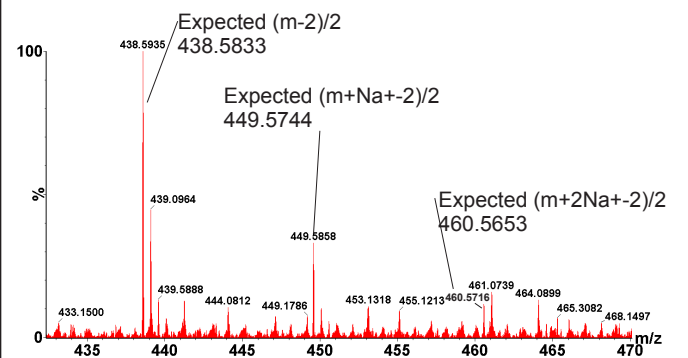
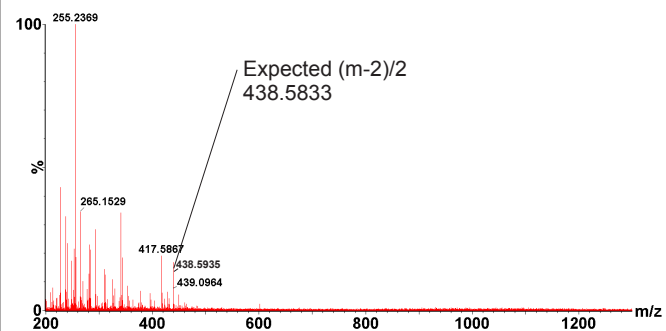


UDP-MurNAc-dipeptide (Ala:Glu)

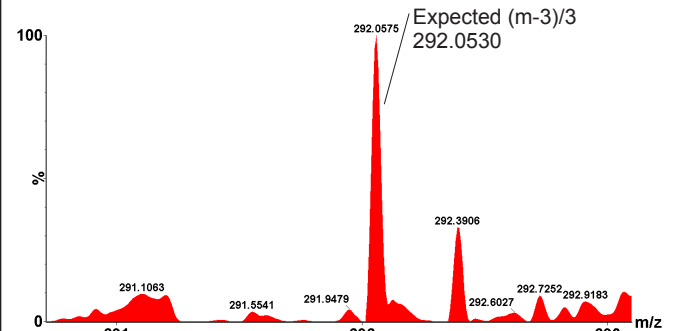
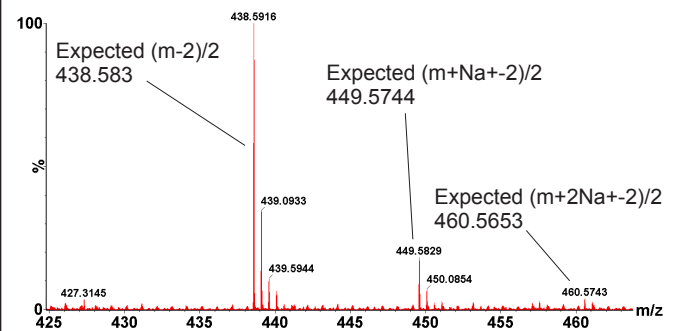
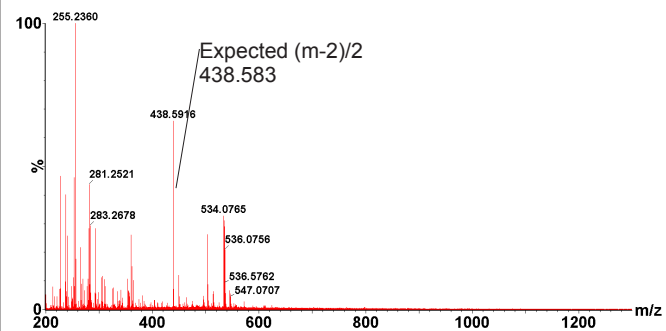
KNOPS D-cycloserine₁₀₀ (C3-4 F23) <https://doi.org/10.1101/2022.01.05.475093>; this version posted January 6, 2022. The copyright holder for this preprint (which was not certified by peer review) is the author/funder, who has granted bioRxiv a license to display the preprint in perpetuity. It is made available under aCC-BY-NC-ND 4.0 International license.



KNOPS + D-cycloserine₁₀₀ (C3-4 F24-25)

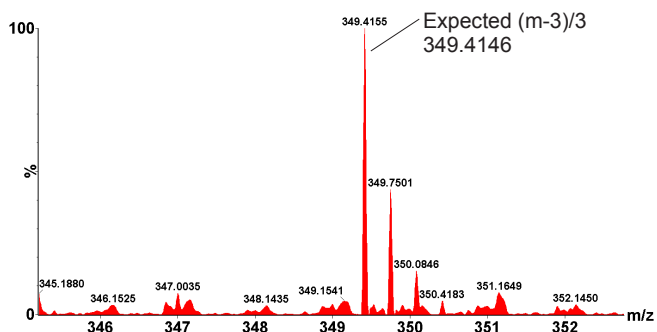
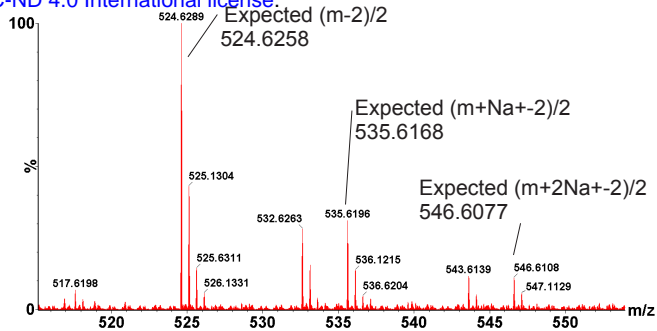
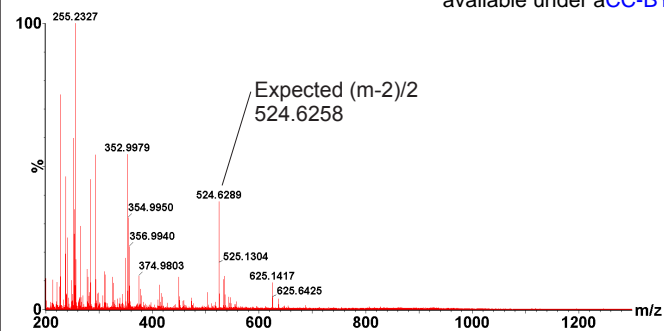


KNOPS +Cb₁₀₀ (C7-8 F23)

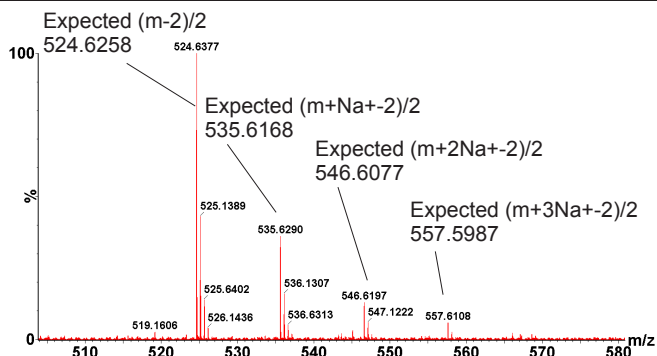
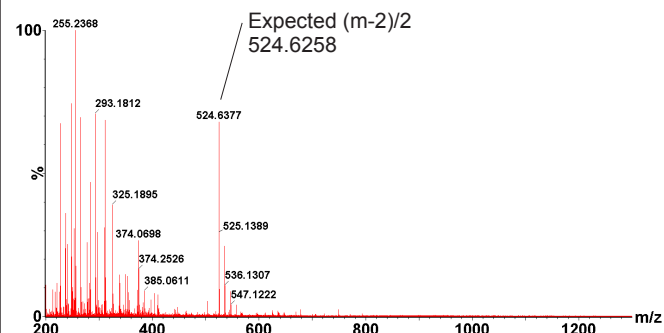


UDP-MurNAc-tripeptide (Ala:Glu:DAP)

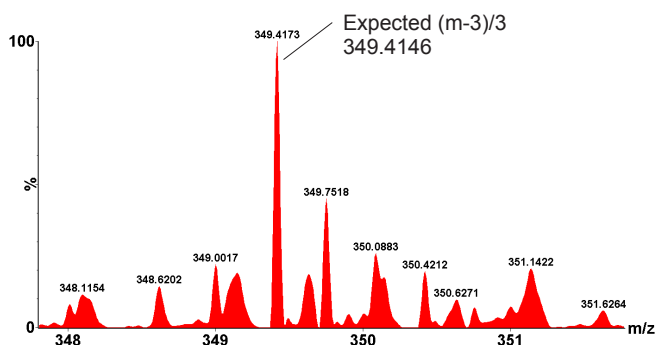
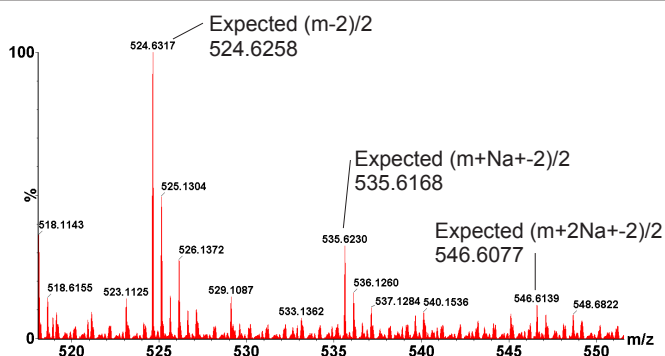
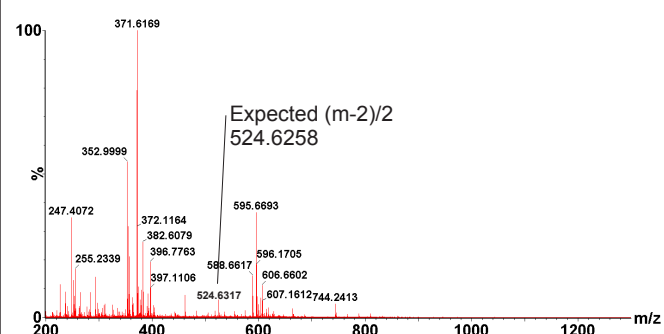
KNOPS + C₇-C₈-F₂₀ <https://doi.org/10.1101/2022.01.05.475093>; this version posted January 6, 2022. The copyright holder for this preprint (which was not certified by peer review) is the author/funder, who has granted bioRxiv a license to display the preprint in perpetuity. It is made available under aCC-BY-NC-ND 4.0 International license.



KNOPS + D-cycloserine₁₀₀ (C3-4 F20)

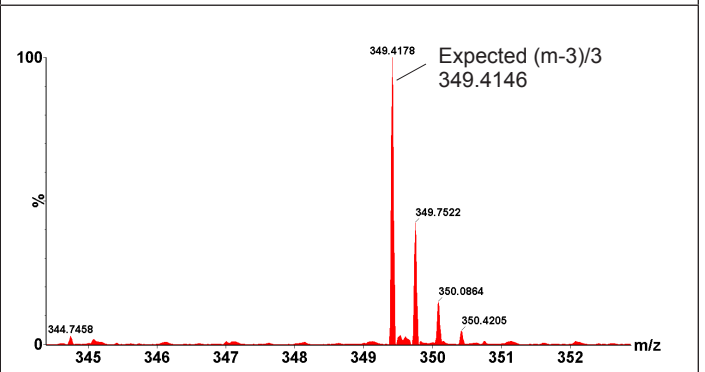
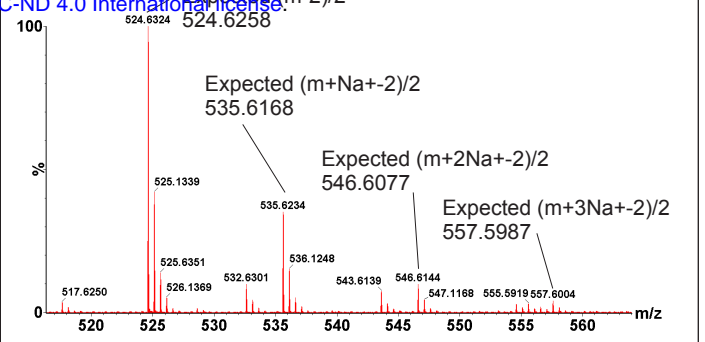
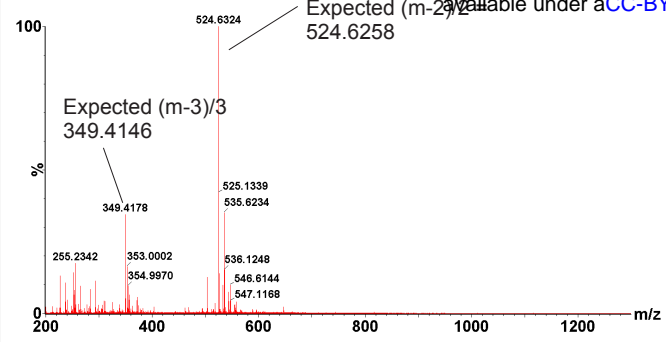


KNOPS + Cb₁₀₀ (C7-8 F19)



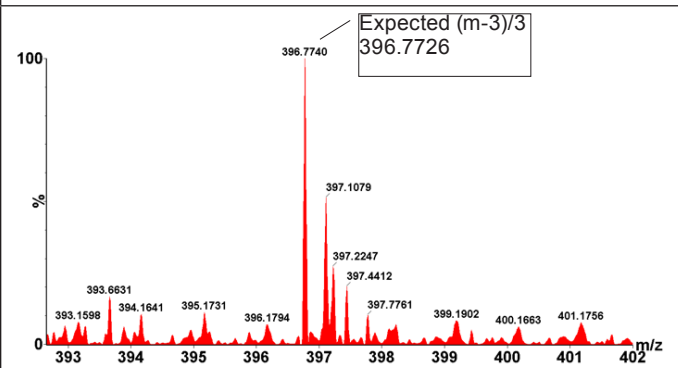
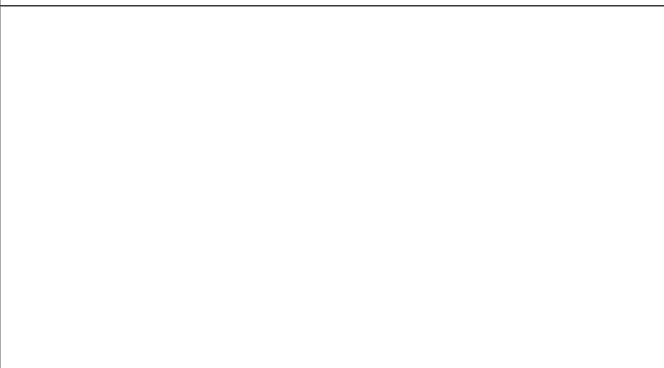
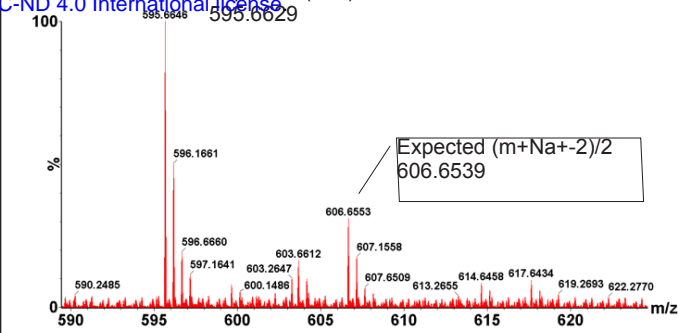
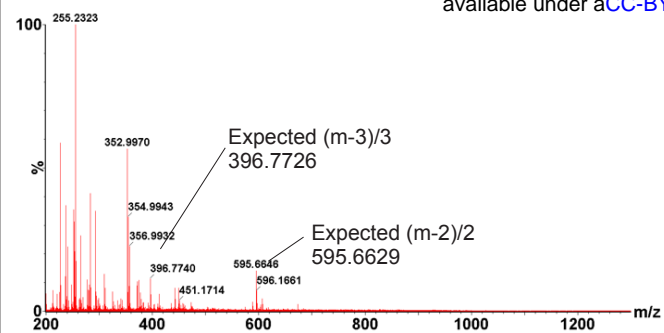
UDP-MurNAc-tripeptide (Ala:Glu:DAP)

KNORR, R. (2022) *bioRxiv preprint doi: <https://doi.org/10.1101/2022.01.05.475093>; this version posted January 6, 2022. The copyright holder for this preprint (which was not certified by peer review) is the author/funder, who has granted bioRxiv a license to display the preprint in perpetuity. It is made available under aCC-BY-NC-ND 4.0 International license.*

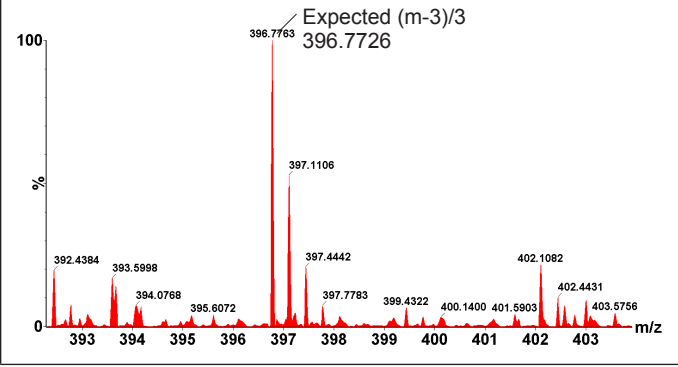
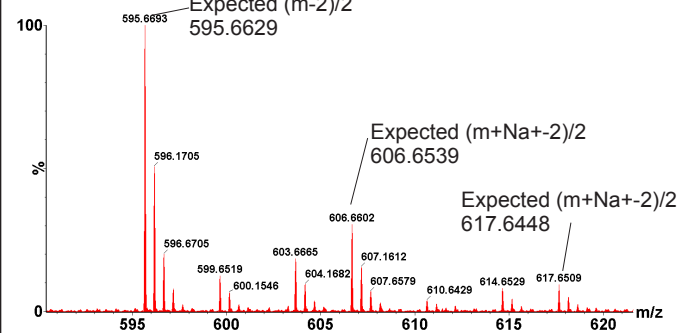
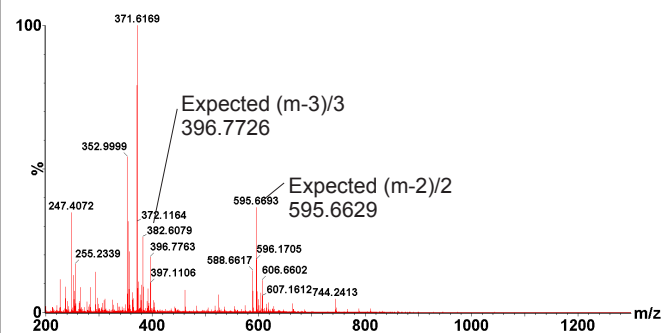


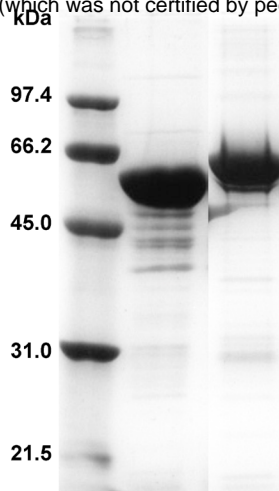
UDP-MurNAc-pentapeptide (Ala:Glu:DAP:Ala:Ala)

KNOPS +C₇C₈F₁₈I₉
 bioRxiv preprint doi: <https://doi.org/10.1101/2022.01.05.475093>; this version posted January 6, 2022. The copyright holder for this preprint (which was not certified by peer review) is the author/funder, who has granted bioRxiv a license to display the preprint in perpetuity. It is made available under aCC-BY-NC-ND 4.0 International license.

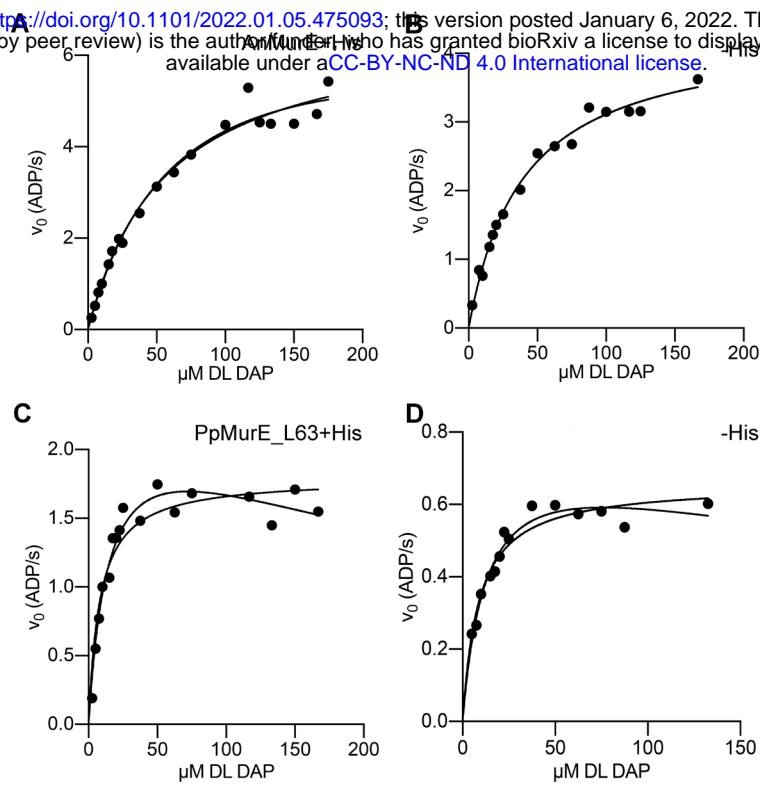


KNOPS +C₁₀₀ (C7-8 F19)

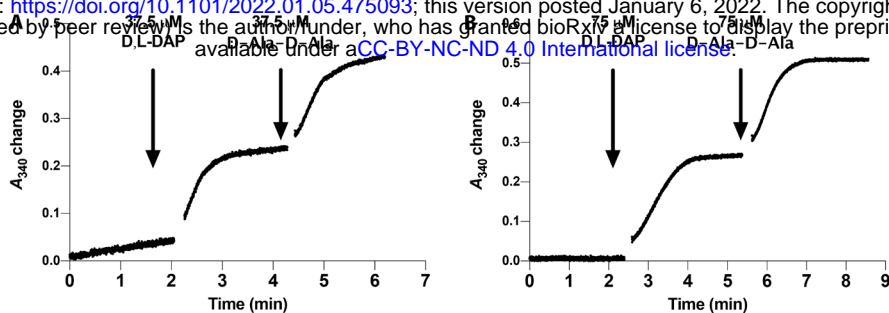




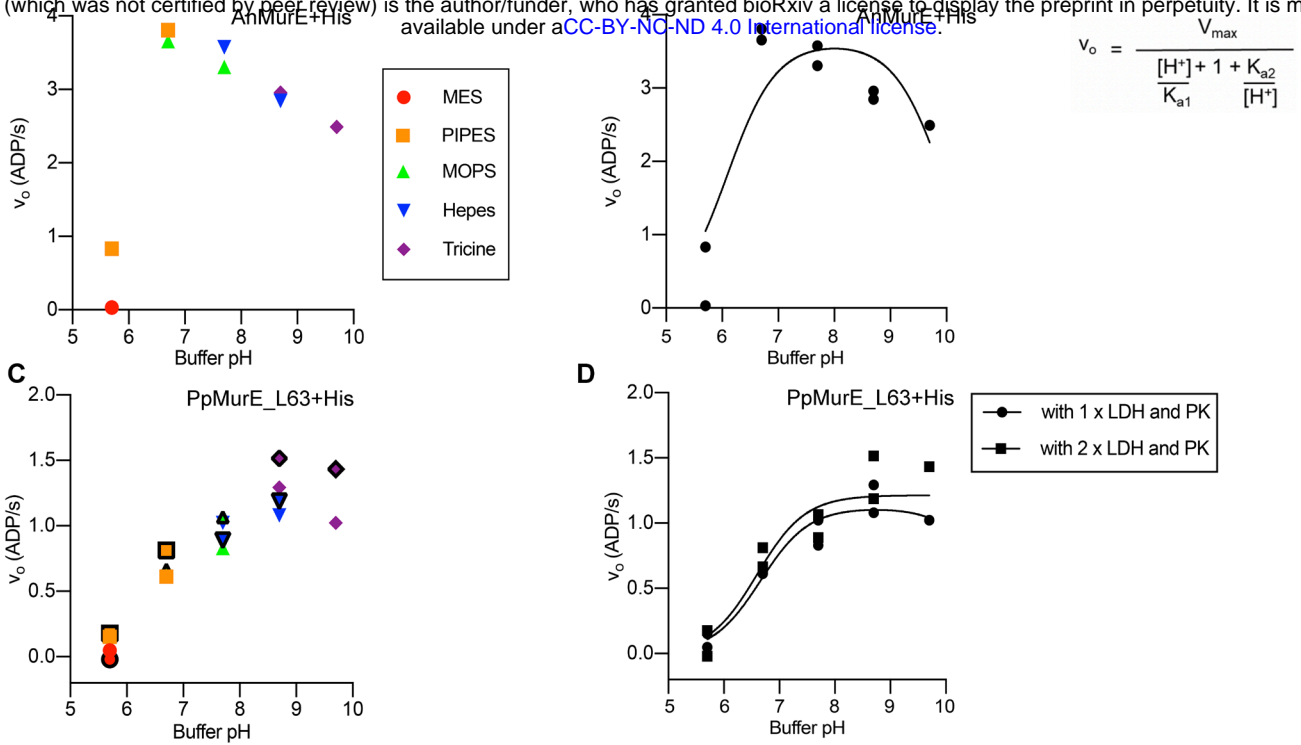
Supplemental Figure S3 PAGE gel of AnMurE and PpMurE_L63 after gel filtration. Lane 1, protein size marker, 2, AnMurE (predicted mass 56.57 kDa) and 3, PpMurE_L63 (predicted mass 62.59 kDa).



Supplemental Figure 4 D,L-DAP substrate curves for AnMurE (A,B) and PpMurE_L63 (C,D). A and C, substrate curves for AnMurE and PpMurE with His tags, at 50 nM and 146 nM, respectively. B and D, substrate curves for AnMurE and PpMurE_L63 after His tags have been cleaved by TEV protease, at 76 nM and 328 nM respectively. Assays were with 1 mM UDP-MurNAc-dipeptide in 50 mM PIPES pH 6.7 (AnMurE) or 50 mM Tricine pH 8.7 (PpMurE_L63). Rates (v_0) in $\text{ADP}\cdot\text{s}^{-1}$ are $\text{mols ADP}\cdot\text{mol Mur ligase}^{-1}\cdot\text{s}^{-1}$. Data show Michaelis Menten curves superimposed on those for substrate inhibition and indicate best fit to Michaelis Menten kinetics for AnMurE and to substrate inhibition for PpMurE_L63 (R^2 values for Michaelis Menten and substrate inhibition are in Figure 4, B).



Supplemental Figure S5 Assay data demonstrating PaMurF utilises the product of AnMurE and PpMurE_L63. A, AnMurE and B, PpMurE_L63. Change in NADH absorbance at A_{340} is coupled to the release of ADP by the MurE and MurF ligases on addition of their substrates D,L-DAP and D-Ala-D-Ala, respectively. Assays included 492 nM PaMurF in 50 mM Hepes, pH 7.6, 375 μ M UDP-MurNAc-dipeptide and A, 100 nM AnMurE+His or B, 300 nM PpMurE_L63+His.



Supplemental Figure S6 Activities of AnMurE and PpMurE_L63 with pH and buffer. Data are presented in two ways: A and C, with coloured symbols to indicate buffers (see legend) and B and D, with non-linear fit to estimate pH optima. Assays for A and B, AnMurE+His and C and D, PpMurE_L63+His, respectively, were in 50 mM buffers in the pH range 5.7-9.7. For PpMurE_L63 C, symbols with black outlines and D, square symbols represent assays with the coupling enzymes lactate dehydrogenase (LDH) and pyruvate kinase (PK) at double the normal concentration (see materials and method), to confirm these were not limiting. Assays included 260 μ M UDPMurNAc-dipeptide and 150 μ M D,L-DAP. If we make the assumption that the only variable responsible for a change in enzyme activity over the pH range tested is the change in $[H^+]$ we can derive an equation that follows the relationship of activity *versus* pH (E) where K_{a1} and K_{a2} are dissociation constants of ionizable groups responsible for the ascending and descending limbs of the pH profile. Data indicate that the pH optima for AnMurE and PpMurE_L63 are 7.5 and 7.5-8.5 respectively.

Enzyme	Source	K_{cat} (s^{-1})	K_m (μM)	$catK_m$ ($s^{-1} \mu M^{-1}$)
AnMurE+His ^{D,L-DAP}	This paper	6.75	56.9	119
AnMurE-His ^{D,L-DAP}		4.34	39.4	110
PpMurE_L63+His ^{D,L-DAP}		2.41	15.2	159
PpMurE_L63-His ^{D,L-DAP}		0.793	13.0	61.0
PaMurE ^{D,L-DAP}	(Paradis-Bleau et al., 2009)	22.2	140	160*
CtMurE ^{D,L-DAP}	(Patin et al., 2009)	0.233	23.0	10.1
MtMurE ^{D,L-DAP}	(Munshi et al., 2013)	1.2	69.0	17.4
EcMurE ^{D,L-DAP}	(Patin et al., 2010)	1.24*	40.0	31.1
SaMurE ^{L-Lys}	(Patin et al., 2010)	4.79*	550	8.71
SaMurE ^{L-Lys}	(Ruane et al., 2013)	4.83	550	8.79
TmMurE ^{L-Lys}	(Boniface et al., 2006)	24.6*	2800	10.3
TmMurE ^{D,L-DAP}	(Boniface et al., 2006)	4.38*	4800	0.912

Supplemental Table S7 Comparison of AnMurE and PpMurE_L63 kinetics with published data for other MurE ligases. PaMurE^{D,L-DAP} *Pseudomonas aeruginosa*, CtMurE^{D,L-DAP} *Chlamydia trachomatis*, MtMurE^{D,L-DAP} *Mycobacterium tuberculosis*, EcMurE^{D,L-DAP} *Escherichia coli*, SaMurE^{L-Lys} *Staphylococcus aureus* and TmMurE^{L-Lys} *Thermotoga maritima*. Asterisks indicate where data were extrapolated from the published values.

Boniface A, Bouhss A, Mengin-Lecreux D, Blanot D (2006) The MurE synthetase from *Thermotoga maritima* is endowed with an unusual D-lysine adding activity. *J Biol Chem* 281: 15680-15686

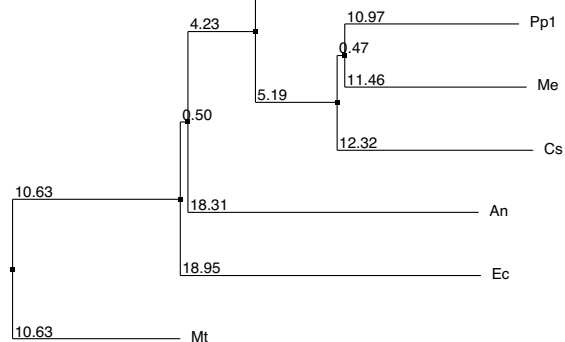
Munshi T, Gupta A, Evangelopoulos D, Guzman JD, Gibbons S, Keep NH, Bhakta S (2013) Characterisation of ATP-dependent Mur ligases involved in the biogenesis of cell wall peptidoglycan in *Mycobacterium tuberculosis*. *PLoS One* 8: e60143

Paradis-Bleau C, Lloyd A, Sanschagrin F, Maaroufi H, Clarke T, Blewett A, Dowson C, Roper DI, Bugg TD, Levesque RC (2009) *Pseudomonas aeruginosa* MurE amide ligase: enzyme kinetics and peptide inhibitor. *Biochem J* 421: 263-272

Patin D, Boniface A, Kovac A, Herve M, Dementin S, Barreteau H, Mengin-Lecreux D, Blanot D (2010) Purification and biochemical characterization of Mur ligases from *Staphylococcus aureus*. *Biochimie* 92: 1793-1800

Patin D, Bostock J, Blanot D, Mengin-Lecreux D, Chopra I (2009) Functional and biochemical analysis of the *Chlamydia trachomatis* ligase MurE. *J Bacteriol* 191: 7430-7435

Ruane KM, Lloyd AJ, Fulop V, Dowson CG, Barreteau H, Boniface A, Dementin S, Blanot D, Mengin-Lecreux D, Gobec S, Dessen A, Roper DI (2013) Specificity determinants for lysine incorporation in *Staphylococcus aureus* peptidoglycan as revealed by the structure of a MurE enzyme ternary complex. *J Biol Chem* 288: 33439-33448



Supplemental Figure S8 Neighbour joining phylogram of MurE of Gram negative bacteria and early plant species, computed using percentage identity in Jalview. Ec *E. coli* (strain K12), An *Anabaena nostoc* PCC7120, Mt *Mycobacterium tuberculosis*, Pp1 *P. patens* (Pp3c24_18820V3.2 v3.3 from Phytozome), Me *Mesotaenium endlicherianum* (WDCW from Onekp CNGDB), Cs *Coleochaete scutata* (VQBJ from Onekp), Gb *Gemmatimonadetes bacterium*. All sequences are from the Uniprot or NCBI databases unless stated otherwise.



Supplemental Figure S9 Clustal Omega (EMBL-EBI)(Madeira et al., 2019) multiple sequence alignment of MurE homologs displayed using Jalview (Waterhouse et al., 2009) with Clustalx designated colours: Sp *Streptococcus pneumoniae*, Sa *Staphylococcus aureus*, Mt *Mycobacterium tuberculosis*, Pp1 *P. patens* (Pp3c24_18820V3.2 v3.3 from Phytosome), Tm *Thermotoga maritima*, Me *Mesotaneium endlicherianum* (WDCW from Onkep CNGDBD), Ec *E. coli* (strain K12), An *Anabaena nostoc* PCC7120. All sequences are from the Uniprot or NCBI databases unless stated otherwise. Green arrows indicate ChloroP predicted cleavage site for PpMurE and red arrows the domain hinge points (Smith, 2010). Black arrows indicate residues with a reported role in MtMurE catalysis (Basavannacharya et al 2010). Letter labels indicate numbered residues with published ligand interactions: ^{Ec} for EcMurE (Gordon et al., 2001), ^{Mt} for MtMurE (Basavannacharya et al., 2010; Maitra et al., 2019) and ^{Sa} for SaMurE (Ruane et al., 2013) with colours indicating binding to UDP (blue), MurNAc sugar (green), ATP or ADP (mauve) and DL-DAP (orange) ligands. Blue asterisks indicate residues common to the Mur ligase family, which includes folypolyglutamate synthetase, cyanophycin synthetase and the capB enzyme from Bacillales (Gordon et al., 2001; Smith, 2010) and pink asterisks indicate residues common to MurC, D, E and F ligases (Basavannacharya et al., 2010). Two streptophyte-specific features are identified by black boxes and the DNPR consensus by a red box.

Basavannacharya C, Moody PR, Munshi T, Cronin N, Keep NH, Bhakta S (2010) Essential residues for the enzyme activity of ATP-dependent MurE ligase from *Mycobacterium tuberculosis*. Protein Cell 1: 1011-1022

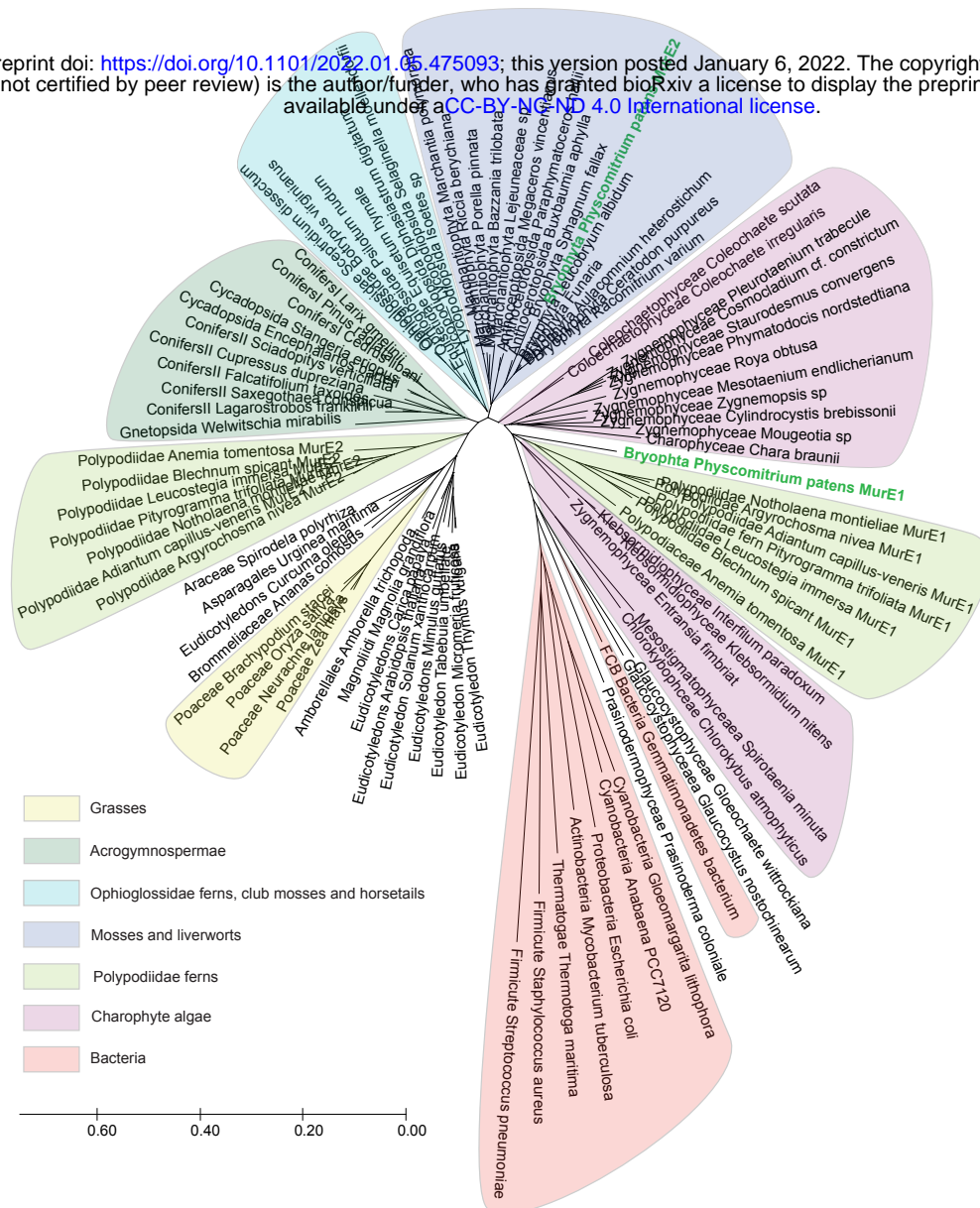
Gordon E, Flouret B, Chantalat L, van Heijenoort J, Mengin-Lecreulx D, Dideberg O (2001) Crystal structure of UDP-N-acetylmuramoyl-L-alanyl-D-glutamate: meso-diaminopimelate ligase from *Escherichia coli*. J Biol Chem 276: 10999-11006

Maitra A, Munshi T, Healy J, Martin LT, Vollmer W, Keep NH, Bhakta S (2019) Cell wall peptidoglycan in *Mycobacterium tuberculosis*: An Achilles' heel for the TB-causing pathogen. FEMS Microbiol Rev 43: 548-575

Ruane KM, Lloyd AJ, Fulop V, Dowson CG, Barreteaou H, Boniface A, Dementin S, Blanot D, Mengin-Lecreulx D, Gobec S, Dessen A, Roper DI (2013) Specificity determinants for lysine incorporation in *Staphylococcus aureus* peptidoglycan as revealed by the structure of a MurE enzyme ternary complex. J Biol Chem 288: 33439-33448

Smith CA (2006) Structure, function and dynamics in the mur family of bacterial cell wall ligases. J Mol Biol 362: 640-655

Waterhouse AM, Procter JB, Martin DM, Clamp M, Barton GJ (2009) Jalview Version 2--a multiple sequence alignment editor and analysis workbench. Bioinformatics 25: 1189-1191



Supplemental Figure S10 Evolutionary relationship of both PpMurE proteins to selected MurE homologs. *P. patens*, as well as many ferns in the Polypodiidae, encodes two MurE homologs: PpMurE1 and PpMurE2, labelled in green. Different taxonomic groups are boxed to highlight the relationship of the *P. patens* proteins to bacterial, algal and streptophyte phyla. Sequences, except *P. patens*, were sourced from the ONEKP database and selected to represent each group (Leebens-Mack et al 2019, Carpenter et al 2019). The evolutionary history was inferred using the Minimum Evolution method (Rzhetsky and Nei, 1992) and computed using MegaX software (Kumar et al 2018). The evolutionary distances, are in the units of the number of amino acid substitutions per site. PpMurE1 and the shorter Polypodiidae fern 'MurE1' homologs are evolutionarily closer to charophyte algae than land plants. PpMurE2 is closer to most marchantiophytes and other bryophytes, which lack a second MurE homolog, whereas the longer Polypodiidae 'MurE2' are closer to the Acrogymnospermae (conifers).

PpMurE2 primarily differs from PpMurE1 in comprising a long, relatively unstructured extension at the amino terminus and a short carboxy terminal extension. The former is considerably longer than a conventional transit peptide (290 residues longer than typical bacterial homologs, compared to 94 residues for PpMurE1) and is common to most seed plant MurE-like proteins, as well as some streptophyte algal and bryophyte MurE homologs. The extended amino terminus is typically proline-rich in the amino terminal residues, being more glycine-rich in lower orders, and, in the later residues, more conserved within different plant divisions. The carboxy terminal extension (24 residues in PpMurE2 beyond a consensus streptophyte DDREECREAL motif in PpMurE1 (Supplemental Figure S9) is more highly conserved, with a consensus sequence (DDREECREALQXVDLHXAGIDTFESPWRXPESX) that is common to most streptophyte MurE homologs, although streptophyte algae lack the terminal PESX. However, where there are two distinct MurE homologs, as there are for *P. patens* and some ferns, this carboxy terminal extension is typically absent from the shorter MurE homologs and these proteins appear to have de-evolved to more closely resemble their bacterial counterparts. The retention of a DNPR motif is common not only to the non-seed plants but also most seed plant MurE homologs, with the similarly charged DNPK also being common, and the Poaceae and a few Pinaceae being notable exceptions (DNPA and DNSR, respectively). In contrast to *P. patens* and the Polypodiidae ferns, many in the same and closely related phyla, including the Acrogymnospermae (Lin et al., 2017) do not have two candidate MurE homologs yet they encode most of the peptidoglycan synthesis enzymes.

Carpenter EJ, Matasci N, Ayyampalayam S, Wu S, Sun J, Yu J, Jimenez Vieira FR, Bowler C, Dorrell RG, Gitzendanner MA, Li L, Du W, K KU, Wickett NJ, Barkmann TJ, Barker MS, Leebens-Mack JH, Wong GK (2019) Access to RNA-sequencing data from 1,173 plant species: The 1000 Plant transcriptomes initiative (1KP). *Gigascience* 8: 1-7

Kumar S, Stecher G, Li M, Knyaz C, Tamura K (2018) MEGA X: Molecular Evolutionary Genetics Analysis across Computing Platforms. *Mol Biol Evol* 35: 1547-1549

Leebens-Mack JH et al., (2019) One thousand plant transcriptomes and the phylogenomics of green plants. *Nature* 574: 679-685

Rzhetsky A, Nei M (1992) Statistical properties of the ordinary least-squares, generalized least-squares, and minimum-evolution methods of phylogenetic inference. *Journal of Molecular Evolution* 35: 367-375

Lin X, Li N, Kudo H, Zhang Z, Li J, Wang L, Zhang W, Takechi K, Takano H (2017) Genes Sufficient for Synthesizing Peptidoglycan are Retained in Gymnosperm Genomes, and MurE from *Larix gmelinii* can Rescue the Albino Phenotype of *Arabidopsis* MurE Mutation. *Plant Cell Physiol* 58: 587-597

Parsed Citations

The authors thank Professor Hiroyoshi Takano (Kumamoto University, Japan) for kindly providing the pTFH22.4 vectors with Anabaena (PCC7120 Q8YWF0|MURE_NOSS1) and P.patens (Pp3c23_15810V3.2) MurE cDNA and Dr Sven Gould (Heinrich Heine University, Düsseldorf, Germany) for helpful discussion on chloroplast evolution. We are also grateful to Julie Tod and Anita Catherwood (University of Warwick, UK) for synthesis of UPD-MurNAc-dipeptide, -tripeptide and -pentapeptide and providing Streptococcus pneumoniae MurE and Pseudomonas aeruginosa MurF and Ian Hands-Portman for access to and training in the School of Life Sciences Imaging Suite, University of Warwick, UK). We also gratefully acknowledge Prof. Rebecca Goss (St Andrews, UK) for provision of pacidamycin.

Barreteau H, Kovac A, Boniface A, Sova M, Gobec S, Blanot D (2008) Cytoplasmic steps of peptidoglycan biosynthesis. FEMS Microbiol Rev 32: 168-207

Google Scholar: [Author Only](#) [Title Only](#) [Author and Title](#)

Blewett AM, Lloyd AJ, Echalié A, Fulop V, Dowson CG, Bugg TD, Roper DI (2004) Expression, purification, crystallization and preliminary characterization of uridine 5'-diphospho-N-acetylmuramoyl L-alanyl-D-glutamate:lysine ligase (MurE) from Streptococcus pneumoniae 110K/70. Acta Crystallogr D Biol Crystallogr 60: 359-361

Google Scholar: [Author Only](#) [Title Only](#) [Author and Title](#)

Boniface A, Bouhss A, Mengin-Lecreux D, Blanot D (2006) The MurE synthetase from Thermotoga maritima is endowed with an unusual D-lysine adding activity. J Biol Chem 281: 15680-15686

Google Scholar: [Author Only](#) [Title Only](#) [Author and Title](#)

Catherwood AC, Lloyd AJ, Tod JA, Chauhan S, Slade SE, Walkowiak GP, Galley NF, Puneekar AS, Smart K, Rea D, Evans ND, Chappell MJ, Roper DI, Dowson CG (2020) Substrate and Stereochemical Control of Peptidoglycan Cross-Linking by Transpeptidation by Escherichia coli PBP1B. J Am Chem Soc 142: 5034-5048

Google Scholar: [Author Only](#) [Title Only](#) [Author and Title](#)

Dagan T, Roettger M, Stucken K, Landan G, Koch R, Major P, Gould SB, Goremykin W, Rippka R, Tandeau de Marsac N, Gugger M, Lockhart PJ, Allen JF, Brune I, Maus I, Puhler A, Martin WF (2013) Genomes of Stigonematalean cyanobacteria (subsection V) and the evolution of oxygenic photosynthesis from prokaryotes to plastids. Genome Biol Evol 5: 31-44

Google Scholar: [Author Only](#) [Title Only](#) [Author and Title](#)

Davis KM, Weiser JN (2011) Modifications to the peptidoglycan backbone help bacteria to establish infection. Infect Immun 79: 562-570

Google Scholar: [Author Only](#) [Title Only](#) [Author and Title](#)

De Benedetti S, Buhl H, Gaballah A, Klockner A, Otten C, Schneider T, Sahl HG, Henrichfreise B (2014) Characterization of serine hydroxymethyltransferase GlyA as a potential source of D-alanine in Chlamydia pneumoniae. Front Cell Infect Microbiol 4: 19

Google Scholar: [Author Only](#) [Title Only](#) [Author and Title](#)

Dementin S, Bouhss A, Auger G, Parquet C, Mengin-Lecreux D, Dideberg O, van Heijenoort J, Blanot D (2001) Evidence of a functional requirement for a carbamoylated lysine residue in MurD, MurE and MurF synthetases as established by chemical rescue experiments. Eur J Biochem 268: 5800-5807

Google Scholar: [Author Only](#) [Title Only](#) [Author and Title](#)

Donoghue P, Paps J (2020) Plant Evolution: Assembling Land Plants. Curr Biol 30: R81-R83

Google Scholar: [Author Only](#) [Title Only](#) [Author and Title](#)

Emanuelsson O, Nielsen, H., von Heijne, G. (1999) ChloroP. Protein Science 8: 978-984

Google Scholar: [Author Only](#) [Title Only](#) [Author and Title](#)

Garcia M, Myouga F, Takechi K, Sato H, Nabeshima K, Nagata N, Takio S, Shinozaki K, Takano H (2008) An Arabidopsis homolog of the bacterial peptidoglycan synthesis enzyme MurE has an essential role in chloroplast development. Plant J 53: 924-934

Google Scholar: [Author Only](#) [Title Only](#) [Author and Title](#)

Higuchi H, Takechi K, Takano H (2016) Visualization of Cyanelle Peptidoglycan in Cyanophora paradoxa Using a Metabolic Labeling Method with Click Chemistry. Cytologia 81: 357-358

Google Scholar: [Author Only](#) [Title Only](#) [Author and Title](#)

Hirano T, Tanidokoro K, Shimizu Y, Kawarabayasi Y, Ohshima T, Sato M, Tadano S, Ishikawa H, Takio S, Takechi K, Takano H (2016) Moss Chloroplasts Are Surrounded by a Peptidoglycan Wall Containing D-Amino Acids. Plant Cell 28: 1521-1532

Google Scholar: [Author Only](#) [Title Only](#) [Author and Title](#)

Hoiczuk E, Hansel A (2000) Cyanobacterial cell walls: news from an unusual prokaryotic envelope. J Bacteriol 182: 1191-1199

Google Scholar: [Author Only](#) [Title Only](#) [Author and Title](#)

Horn S, Takechi K, Tanidokoro K, Sato H, Takio S, Takano H (2009) The peptidoglycan biosynthesis genes MurA and MraY are related to chloroplast division in the moss Physcomitrella patens. Plant Cell Physiol 50: 2047-2056

Google Scholar: [Author Only](#) [Title Only](#) [Author and Title](#)

Huber R, Langworthy, T. A., König, H., Thomm, M., Woese, C.R., Sleytr, U.B. and Stetter, K. O. (1986) *Thermotoga maritima* sp. nov. represents a new genus of unique extremely thermophilic eubacteria *Arch. Microbiol.* 144: 324-333

Google Scholar: [Author Only](#) [Title Only](#) [Author and Title](#)

Hudson AO, Singh BK, Leustek T, Gilvarg C (2006) An LL-diaminopimelate aminotransferase defines a novel variant of the lysine biosynthesis pathway in plants. *Plant Physiol* 140: 292-301

Google Scholar: [Author Only](#) [Title Only](#) [Author and Title](#)

Izumi Y, Kuroki J, Nagafuji H, Lin X, Takano H (2008) Effects of antibiotics that inhibit bacterial peptidoglycan synthesis on plastid division in pteridophytes. *Cytologia* 73: 393-400

Google Scholar: [Author Only](#) [Title Only](#) [Author and Title](#)

Jurgens UJ, Drews G, Weckesser J (1983) Primary structure of the peptidoglycan from the unicellular cyanobacterium *Synechocystis* sp. strain PCC 6714. *J Bacteriol* 154: 471-478

Google Scholar: [Author Only](#) [Title Only](#) [Author and Title](#)

Kasten B, Reski R (1997) β -Lactam antibiotics inhibit chloroplast division in a moss (*Physcomitrella patens*) but not in tomato (*Lycopersicon esculentum*). *Journal of Plant Physiology* 150: 137-140

Google Scholar: [Author Only](#) [Title Only](#) [Author and Title](#)

Katayama N, Takano H, Sugiyama M, Takio S, Sakai A, Tanaka K, Kuroiwa H, Ono K (2003) Effects of antibiotics that inhibit the bacterial peptidoglycan synthesis pathway on moss chloroplast division. *Plant Cell Physiol* 44: 776-781

Google Scholar: [Author Only](#) [Title Only](#) [Author and Title](#)

Kolukisaoglu Ü, Suarez J (2017) D-Amino Acids in Plants: New Insights and Aspects, but also More Open Questions. In *Amino Acid - New Insights and Roles in Plant and Animal*,

Google Scholar: [Author Only](#) [Title Only](#) [Author and Title](#)

Lang D, Ullrich KK, Murat F, Fuchs J, Jenkins J, Haas FB, Piednoel M, Gundlach H, Van Bel M, Meyberg R, Vives C, Morata J, Symeonidi A, Hiss M, Muchero W, Kamisugi Y, Saleh O, Blanc G, Decker EL, van Gessel N, Grimwood J, Hayes RD, Graham SW, Gunter LE, McDaniel SF, Hoernstein SNW, Larsson A, Li FW, Perroud PF, Phillips J, Ranjan P, Rokshar DS, Rothfels CJ, Schneider L, Shu S, Stevenson DW, Thummel F, Tillich M, Villarreal Aguilar JC, Widiez T, Wong GK, Wymore A, Zhang Y, Zimmer AD, Quatrano RS, Mayer KFX, Goodstein D, Casacuberta JM, Vandepoele K, Reski R, Cuming AC, Tuskan GA, Maumus F, Salse J, Schmutz J, Rensing SA (2018) The *Physcomitrella patens* chromosome-scale assembly reveals moss genome structure and evolution. *Plant J* 93: 515-533

Google Scholar: [Author Only](#) [Title Only](#) [Author and Title](#)

Lin X, Li N, Kudo H, Zhang Z, Li J, Wang L, Zhang W, Takechi K, Takano H (2017) Genes Sufficient for Synthesizing Peptidoglycan are Retained in Gymnosperm Genomes, and MurE from *Larix gmelinii* can Rescue the Albino Phenotype of *Arabidopsis* MurE Mutation. *Plant Cell Physiol* 58: 587-597

Google Scholar: [Author Only](#) [Title Only](#) [Author and Title](#)

Machida M, Takechi K, Sato H, Chung SJ, Kuroiwa H, Takio S, Seki M, Shinozaki K, Fujita T, Hasebe M, Takano H (2006) Genes for the peptidoglycan synthesis pathway are essential for chloroplast division in moss. *Proceedings of the National Academy of Sciences* 103: 6753-6758

Google Scholar: [Author Only](#) [Title Only](#) [Author and Title](#)

Majce V, Ruane KM, Gobec S, Roper DI (2013) Crystallization and preliminary X-ray analysis of a UDP-MurNAc-tripeptide D-alanyl-D-alanine-adding enzyme (PaMurF) from *Pseudomonas aeruginosa*. *Acta Crystallogr Sect F Struct Biol Cryst Commun* 69: 503-505

Google Scholar: [Author Only](#) [Title Only](#) [Author and Title](#)

Matsumoto H, Takechi K, Sato H, Takio S, Takano H (2012) Treatment with antibiotics that interfere with peptidoglycan biosynthesis inhibits chloroplast division in the desmid *Closterium*. *PLoS One* 7: e40734

Google Scholar: [Author Only](#) [Title Only](#) [Author and Title](#)

Mengin-Lecreux D, Flouret B, van Heijenoort J (1982) Cytoplasmic steps of peptidoglycan synthesis in *Escherichia coli*. *J Bacteriol* 151: 1109-1117

Google Scholar: [Author Only](#) [Title Only](#) [Author and Title](#)

Packiam M, Weinrick B, Jacobs WR, Jr., Maurelli AT (2015) Structural characterization of muropeptides from *Chlamydia trachomatis* peptidoglycan by mass spectrometry resolves "chlamydial anomaly". *Proc Natl Acad Sci U S A* 112: 11660-11665

Google Scholar: [Author Only](#) [Title Only](#) [Author and Title](#)

Pfanzagl B, Allmaier G, Schmid ER, A DPM, Löffelhardt W (1996) N-Acetylputrescine as a Characteristic Constituent of *Cyanella* Peptidoglycan in Glaucocystophyte Algae. *Journal of Bacteriology* 178: 6994-6997

Google Scholar: [Author Only](#) [Title Only](#) [Author and Title](#)

Ponce-Toledo RI, Deschamps P, Lopez-Garcia P, Zivanovic Y, Benzerara K, Moreira D (2017) An Early-Branching Freshwater

Cyanobacterium at the Origin of Plastids. *Curr Biol* 27: 386-391

Google Scholar: [Author Only](#) [Title Only](#) [Author and Title](#)

Rensing SA, Lang D, Zimmer AD, Terry A, Salamov A, Shapiro H, Nishiyama T, Perroud PF, Lindquist EA, Kamisugi Y, Tanahashi T, Sakakibara K, Fujita T, Oishi K, Shin IT, Kuroki Y, Toyoda A, Suzuki Y, Hashimoto S, Yamaguchi K, Sugano S, Kohara Y, Fujiyama A, Anterola A, Aoki S, Ashton N, Barbazuk WB, Barker E, Bennetzen JL, Blankenship R, Cho SH, Dutcher SK, Estelle M, Fawcett JA, Gundlach H, Hanada K, Heyl A, Hicks KA, Hughes J, Lohr M, Mayer K, Melkozernov A, Murata T, Nelson DR, Pils B, Prigge M, Reiss B, Renner T, Rombauts S, Rushton PJ, Sanderfoot A, Schween G, Shiu SH, Stueber K, Theodoulou FL, Tu H, Van de Peer Y, Verrier PJ, Waters E, Wood A, Yang L, Cove D, Cuming AC, Hasebe M, Lucas S, Mishler BD, Reski R, Grigoriev IV, Quatrano RS, Boore JL (2008) The *Physcomitrella* genome reveals evolutionary insights into the conquest of land by plants. *Science* 319: 64-69

Google Scholar: [Author Only](#) [Title Only](#) [Author and Title](#)

Roten CA, Brandt C, Karamata D (1991) Genes involved in meso-diaminopimelate synthesis in *Bacillus subtilis*: identification of the gene encoding aspartokinase I. *J Gen Microbiol* 137: 951-962

Google Scholar: [Author Only](#) [Title Only](#) [Author and Title](#)

Ruane KM, Lloyd AJ, Fulop V, Dowson CG, Barreteau H, Boniface A, Dementin S, Blanot D, Mengin-Lecreux D, Gobec S, Dessen A, Roper DI (2013) Specificity determinants for lysine incorporation in *Staphylococcus aureus* peptidoglycan as revealed by the structure of a MurE enzyme ternary complex. *J Biol Chem* 288: 33439-33448

Google Scholar: [Author Only](#) [Title Only](#) [Author and Title](#)

Sato N, Takano H (2017) Diverse origins of enzymes involved in the biosynthesis of chloroplast peptidoglycan. *J Plant Res* 130: 635-645

Google Scholar: [Author Only](#) [Title Only](#) [Author and Title](#)

Sato N, Toyoshima M, Tajima N, Takechi K, Takano H (2017) Single-Pixel Densitometry Revealed the Presence of Peptidoglycan in the Intermembrane Space of the Moss Chloroplast Envelope in Conventional Electron Micrographs. *Plant Cell Physiol* 58: 1743-1751

Google Scholar: [Author Only](#) [Title Only](#) [Author and Title](#)

Schleifer KH, Kandler O (1972) Peptidoglycan. Types of Bacterial Cell Walls and their Taxonomic Implications. *Bacteriological Reviews* 36: 407-477

Google Scholar: [Author Only](#) [Title Only](#) [Author and Title](#)

Schween G, Gorr G, Hohe A, Reski R (2003) Unique Tissue-Specific Cell Cycle in *Physcomitrella*. *Plant Biology* 5: 50-58

Google Scholar: [Author Only](#) [Title Only](#) [Author and Title](#)

Scott OT, Castenholz RW, Bonnett HT (1984) Evidence for a peptidoglycan envelope in the cyanelles of *Glaucozystis nochinearum* Itzigsohn. *Arch Microbiol*. 139: 130-138

Google Scholar: [Author Only](#) [Title Only](#) [Author and Title](#)

Takahashi Y, Takechi K, Takio S, Takano H (2016) Both the transglycosylase and transpeptidase functions in plastid penicillin-binding protein are essential for plastid division in *Physcomitrella patens*. *Proc Jpn Acad Ser B Phys Biol Sci* 92: 499-508

Google Scholar: [Author Only](#) [Title Only](#) [Author and Title](#)

Takano H, Takechi K (2010) Plastid peptidoglycan. *Biochim Biophys Acta* 1800: 144-151

Google Scholar: [Author Only](#) [Title Only](#) [Author and Title](#)

Takano H, Tsunefuka T, Takio S, Ishikawa H, Takechi K (2018) Visualization of Plastid Peptidoglycan in the Charophyte Alga *Klebsormidium nitens* Using a Metabolic Labeling Method. *Cytologia* 83: 375-380

Google Scholar: [Author Only](#) [Title Only](#) [Author and Title](#)

Utsunomiya H, Saiki N, Kadoguchi H, Fukudome M, Hashimoto S, Ueda M, Takechi K, Takano H (2020) Genes encoding lipid II flippase MurJ and peptidoglycan hydrolases are required for chloroplast division in the moss *Physcomitrella patens*. *Plant Mol Biol*

Google Scholar: [Author Only](#) [Title Only](#) [Author and Title](#)

van Baren MJ, Bachy C, Reistetter EN, Purvine SO, Grimwood J, Sudek S, Yu H, Poirier C, Deerinck TJ, Kuo A, Grigoriev IV, Wong CH, Smith RD, Callister SJ, Wei CL, Schmutz J, Worden AZ (2016) Evidence-based green algal genomics reveals marine diversity and ancestral characteristics of land plants. *BMC Genomics* 17: 267

Google Scholar: [Author Only](#) [Title Only](#) [Author and Title](#)

Vollmer W, Blanot D, de Pedro MA (2008) Peptidoglycan structure and architecture. *FEMS Microbiol Rev* 32: 149-167

Google Scholar: [Author Only](#) [Title Only](#) [Author and Title](#)

Williams-Carrier R, Zoschke R, Belcher S, Pfalz J, Barkan A (2014) A major role for the plastid-encoded RNA polymerase complex in the expression of plastid transfer RNAs. *Plant Physiol* 164: 239-248

Google Scholar: [Author Only](#) [Title Only](#) [Author and Title](#)

Woitzik D, Weckesser, J. and Jurgens, U.J. (1988) Isolation and Characterization of Cell Wall Components of the unicellular cyanobacterium synechococcus sp PCC 6301. J. Gen. Microbiol. 134: 619-627

Google Scholar: [Author Only](#) [Title Only](#) [Author and Title](#)

Wolfert MA, Roychowdhury A, Boons GJ (2007) Modification of the structure of peptidoglycan is a strategy to avoid detection by nucleotide-binding oligomerization domain protein 1. Infect Immun 75: 706-713

Google Scholar: [Author Only](#) [Title Only](#) [Author and Title](#)

Zeng Y, Feng F, Medova H, Dean J, Koblizek M (2014) Functional type 2 photosynthetic reaction centers found in the rare bacterial phylum Gemmatimonadetes. Proc Natl Acad Sci U S A 111: 7795-7800

Google Scholar: [Author Only](#) [Title Only](#) [Author and Title](#)